Ph.D. DISSERTATION

WIRELESS INDOOR LOCALIZATION ALGORITHMS FOR INTERNET OF THINGS

사물인터넷을 위한 무선 실내 측위 알고리즘

BY

LEE BYEONG-HO

FEBRUARY 2022

DEPARTMENT OF ELECTRICAL AND
COMPUTER ENGINEERING
COLLEGE OF ENGINEERING
SEOUL NATIONAL UNIVERSITY

Ph.D. DISSERTATION

WIRELESS INDOOR LOCALIZATION ALGORITHMS FOR INTERNET OF THINGS

사물인터넷을 위한 무선 실내 측위 알고리즘

BY

LEE BYEONG-HO

FEBRUARY 2022

DEPARTMENT OF ELECTRICAL AND
COMPUTER ENGINEERING
COLLEGE OF ENGINEERING
SEOUL NATIONAL UNIVERSITY

WIRELESS INDOOR LOCALIZATION ALGORITHMS FOR INTERNET OF THINGS

사물인터넷을 위한 무선 실내 측위 알고리즘

지도교수 김 성 철
이 논문을 공학박사 학위논문으로 제출함

2022년 2월

서울대학교 대학원

전기 · 정보 공학부

이 병 호

이병호의 공학박사 학위 논문을 인준함

2022년 2월

위 원 장:	박세웅	(인)
부위원장:	김성철	(인)
위 원:	조남익	(인)
위 원:	이정규	(인)
위 원:	이성욱	(인)

Abstract

Indoor location-based services (LBS) can be combined with various applications such as indoor navigation for smartphone users, resource management in smart factories, and autonomous driving of robots. It is also indispensable for Internet of Things (IoT) applications. For various LBS, accurate location information is essential. Therefore, a proper ranging and positioning algorithm is important. For outdoors, the global navigation satellite system (GNSS) is available to provide position information. However, the GNSS is inappropriate indoors owing to the issue of the blocking of the signals from satellites. It is necessary to develop a technology that can replace GNSS in GNSS-denied environments. Among the various alternative systems, the one of promising technology is to use a Wi-Fi system that has already been applied to many commercial devices, and the infrastructure is in place in many regions. In this dissertation, Wi-Fi based indoor localization methods are presented. In the specific, I propose the three major issues related to accurate indoor localization using received signal strength (RSS) and fine timing measurement (FTM) protocol in the 802.11 standard for my dissertation topics. First, I propose a hybrid localization algorithm to boost the accuracy of range-based localization by improving the ranging accuracy under indoor non-line-of-sight (NLOS) conditions. I replaced the ranging part of the rule-based localization method with a deep regression model that uses data-driven learning with dual-band received signal strength (RSS). The ranging error caused by the NLOS conditions was effectively reduced by using the deep regression method. As a consequence, the positioning error could be reduced under NLOS conditions. The performance of the proposed method was verified through a ray-tracing-based simulation for indoor spaces. The proposed scheme showed a reduction in the positioning error of at least 22.3% in terms of the median root mean square error. Next, I study on positioning algorithm that considering NLOS conditions for each APs, us-

ing single band RSS measurement. The single band RSS information is widely used for indoor localization because they can be easily implemented by using existing infrastructure like Wi-Fi, Blutooth, or Zigbee. However, range estimation with a single pathloss model produces considerable errors, which degrade the positioning performance. This problem mainly arises because the single pathloss model cannot reflect diverse indoor radio wave propagation characteristics. In this study, I develop a new overlapping multi-state model to consider multiple candidates of pathloss models including line-of-sight (LOS) and NLOS states, and propose an efficient way to select a proper model for each reference node involved in the localization process. To this end, I formulate a cost function whose value varies widely depending on the choice of pathloss model of each access point. Because the computational complexity to find an optimal channel model for each reference node exponentially increases with the number of reference nodes, I apply a genetic algorithm to significantly reduce the complexity so that the proposed method can be executed in real-time. Experimental validations with ray-tracing simulations and RSS measurements at a real site confirm the improvement of localization accuracy for Wi-Fi in indoor environments. The proposed method achieves up to 1.92 m mean positioning error under a practical indoor environment and produces a performance improvement of 31.09% over the benchmark scenario. Finally, I investigate accurate indoor tracking algorithm using FTM protocol in this dissertation. By using the FTM ranging and the built-in sensors in a smartphone, it is possible to track the user's location in indoor. However, the failure of first peak detection due to the multipath effect causes a bias in the FTM ranging results in the practical indoor environment. Additionally, the unexpected ranging error dependent on device type also degrades the indoor positioning accuracy. In this study, I considered the factors of ranging error in the FTM protocol in practical indoor environment, and proposed a method to compensate ranging error. I designed an EKF-based tracking algorithm that adaptively removes outliers from the FTM result and corrects bias

to increase positioning accuracy. The experimental results verified that the proposed algorithm reduces the average ofthe ranging bias by 43-65% in an indoor scenarios, and can achieve the sub-meter accuracy in average route mean squared error of user's position in the experiment scenarios.

keywords: Fine Timing Measurement, Indoor Localization, Range-based Localization, Received Signal Strength, Trilateration, Wi-Fi Positioning
student number: 2015-20965

Contents

List of Tables

List of Figures

Chapter 1

INTRODUCTION

Recently, several studies have been conducted on indoor location-based services (LBS). LBS can be combined with various applications such as navigation for smartphone users, resource management in smart factories, and autonomous driving of robots, surveillance and security, among others. For various LBS, indoor positioning or the so-called localization technique is a core technology. It is also indispensable for Internet of Things services [1–4]. For outdoors, the global navigation satellite system (GNSS) is available to provide position information. However, the GNSS is inappropriate indoors owing to the issue of the blocking of the signals from satellites. Several studies have been conducted in order to estimate locations in GNSS-denied environments. In particular, the method of using the received signal strength (RSS) from Wi-Fi communication is promising because it fits most commercial products [1, 5, 6]. For indoor environments, in which it is difficult to use GNSS, there have been studies that have used various alternative systems to find the locations of devices. There are infrastructureless methods that avoid dependence on a specific infrastructure by measuring a passive signal with a magnetometer, an inertial sensor, a microphone, or a light sensor [7–10]. On the other hand, some localization methods depend on the infrastructure, which takes over the role of the satellites in the GNSS. Some studies used an ultra-wide-band (UWB) tag [11], Bluetooth beacon [12, 13], or radio frequency identification tag [14].

Because these methods have weaker signal strength and smaller coverage than Wi-Fi systems in indoor environment with many walls. In addition, they require a deployment of the infrastructure. Although localization methods that use Wi-Fi also require the placement of Wi-Fi APs, many Wi-Fi APs are already currently deployed. Therefore, localization methods that use Wi-Fi have the advantage of being used without the installation of additional infrastructure compared to other infrastructure-based methods.

Especially for smartphones, studies combining Wi-Fi and the other infrastructureless methods have been conducted. Several state-of-art approaches used a fine timing measurement (FTM) protocol supported by a Wi-Fi system, which is a method of using a measurement of the distance based on the round-trip time by exchanging packets when both the AP and the device support the FTM protocol [15]. In particular, such approaches showed high ranging accuracy under LOS conditions [16, 17], and these studies using a fusion of FTM and other sensors showed high accuracy in tracking the path of a pedestrian [18–20].

To reduce the dependency on infrastructure as much as possible, there are methods that use the RSS of a Wi-Fi beacon's signal. Wi-Fi RSS depends on the indoor wave propagation characteristics, and especially the path-loss properties with respect to the distance. Many studies have been conducted on indoor path loss, which has been integrated into statistical models [21–23]. The ITU-1238 model in [22] assumes the PLM in the indoor environment as a 1-slope model, and presents path loss parameters for several open space and NLOS environments. The models introduced in [21, 23] are based on 2-slope model, considering the complex indoor environment. However, these channel models were used to analyze the quality of service in communication. Range-based localization requires site-specific channel information. In particular, a detailed model of the shadowing effect caused by walls is necessary. In [24], the propagation loss for a common building material in the 2.4 and 5.2 GHz bands was analyzed. In [25], the effects of walls on the propagation loss in complex indoor environments

were analyzed, and an effective wall loss model was proposed.

Meanwhile, most indoor localization studies that use RSS rely on a fingerprint-based method. Existing single-band based fingerprinting techniques [6,26–28] demonstrate good localization accuracy, but require a thorough site survey of the target space. Channel state information (CSI) was also measured in [**?**,27,28]. Fingerprinting methods that use CSI provide high accuracy. However, there is a risk that they may not be robust to AP location changes after a site survey because CSI is sensitive to spatial configurations. In addition, CSI has a high data overhead and can only be acquired with specific devices.

Some studies used dual-band RSS for fingerprint-based positioning [29–34]. Consequently, the accuracy of these methods depends on site surveys, and vulnerable to environmental changes. In [31], rule-based localization was exploited by using dual-band RSS with consideration of NLOS conditions. The channel conditions were evaluated by comparing the RSS attenuation between the two bands, and different ranging functions were applied according to the channel conditions. However, the authors of [31] classified the channel conditions into three types, which were insufficient to reflect indoor channel conditions. The use of deep learning has been attempted in order to overcome the limitations of rule-based methods. The authors of [35–37] estimated positions by training a neural network with RSS vectors from multiple APs. These were types of fingerprint-based methods that derived the location coordinates output from the neural network, which was trained with RSS patterns. Therefore, similarly to other fingerprint-based methods, there was a disadvantage in that they could only operate in a pre-surveyed environment. Previous studies about indoor localization using Wi-Fi RSS with deep learning techniques were mainly based on fingerprinting. The fingerprint-based methods can achieve high positioning accuracy, but require heavy site surveys and are vulnerable to minor environmental changes, such as changes in APs' locations or obstructions. For these reasons, the goal of this dissertation is to present a robust indoor localization methods that minimize the need for site survey. I study on the three

major issues related to accurate indoor localization using RSS and FTM protocol for my dissertation topics. The first issue is about increasing the accuracy of RSS ranging in the indoor environment. In the rang-based localization, the ranging accuracy has a great influence on the location accuracy. In particular, RSS attenuation caused by wall structures and obstacles in the indoor causes a degradation in the ranging accuracy. In this dissertation, I propose a hybrid approach, which applies data-driven deep learning to only the ranging part of a rule-based localization algorithm. This approach has the advantage of being robust against changes in the AP locations and spatial structure. A ray-tracing method was used to get the channel data for a complex NLOS environment, and the ranging performance of the proposed dual-band RSS was evaluated and compared to that of existing methods.

The next issue deals with a positioning algorithm that accurately estimates the location of a device in a complex indoor environment with measurements including dynamic RSS ranging error. The overlapped multi-state PLM which is suitable for location estimation is derived by analyzing RSS measurement in indoor environment where LOS/NLOS states are mixed. When estimating device's position using RSS measurements from multiple APs, I designed an algorithm that accurately finds the optimal PLM state combination for each AP and the location of the target device. To reduce computational complexity to a realistic level, a genetic algorithm (GA) is applied. And, I conducted a numerical analysis via ray-tracing based simulations for indoor environments and with experiments at a general hospital.

Finally, I present a method to improve FTM-based ranging and location tracking accuracy in the indoor environment. I analyzed the distance error characteristic that occurs when the smartphone carried by the pedestrian in the practical indoor environment, and designed an algorithm to compensate the biased FTM ranging result. In the indoor environment, since LOS is hard to be secured due to obstacles, the measured ranging results are prone to be positively biased. In addition, an unexpected error depending on the device types brings about outlier and degrades the tracking accuracy.

These practical ranging errors are the main challenge in accurately tracking the indoor location. I designed an extended Kalman filter (EKF)-based algorithm that adaptively removes outlier and compensates the ranging bias. Measurement experiments were conducted considering non-homogeneous AP set scenarios in an indoor environment, and the performance of the proposed algorithm was evaluated.

Chapter 2

Hybrid Approach for Indoor Localization Using Received Signal Strength of Dual-Band Wi-Fi

2.1 Motivation

Indoor localization technology is indispensable for Internet of Things services. It can be applied to a wide range of fields, such as navigation for smartphone users, resource management in smart factories, and autonomous driving of robots, among others. Outdoors, the global navigation satellite system (GNSS) is available to provide position information. However, the GNSS is inappropriate indoors owing to the issue of the blocking of the signals from satellites. Several studies have been conducted in order to estimate locations in GNSS-denied environments. In particular, the method of using the received signal strength (RSS) from Wi-Fi communication is promising because it fits most commercial products [1, 5, 6].

Indoor localization methods that use RSS can be divided into two groups: fingerprint-based methods and range-based methods [5]. The fingerprint-based methods are based on a pattern-matching scheme. The RSS patterns from multiple access points (APs) at a specific location were recorded in the offline stage. In the online stage, the measured RSS pattern is compared with a recorded database to match a location. The offline

stage requires time and effort for site surveys and is vulnerable to channel changes (e.g., AP location changes and furniture structure changes) [6]. Range-based localization methods estimates the distance between individual APs and a target node and specify a location through geometric inference. The main problem in range-based localization using RSS is the ranging error. The RSS ranging error result from the non-line-of-sight (NLOS) channel condition, antenna direction, and time-varying obstruction by crowds. Among these, the NLOS effect of indoor wall structures and obstacles is the most important factor. The shadowing effect caused by wall structures makes RSS ranging difficult, resulting in position inaccuracy [38, 39].

Therefore, improving the ranging accuracy is a key factor for range-based localization. Typically, RSS ranging is based on a path-loss model (PLM), which represents the relation between the RSS and the distance between communication nodes. The representative model is the two-slope model presented in the IEEE 802.11 standard [21]. This is an expression for an universal indoor space and does not reflect a site-specific environment. Therefore, the ranging accuracy based on this model is limited in practical cases. To solve this problem, studies have been conducted on the adjustment of the parameters of the PLM [40–43] and the correction of ranging results through the detection of NLOS by using RSS changes over time or characteristics of differences in RSS in dual-frequency bands.

The method of adjusting the PLM's parameters to fit into a specific environment improves the statistical ranging accuracy; however, there is a limit to reflecting complex indoor spaces with severe NLOS conditions. The method that uses the time-varying RSS has a disadvantage in terms of time consumption. The dual-band scheme is based on the wave propagation characteristics in an NLOS environment with a carrier frequency. In practice, many off-the-shelf Wi-Fi APs and mobile devices are compatible with dual-band operation.

In addition, many approaches use deep learning techniques. Most localization algorithms that use deep learning can be regarded as data-driven methods, as they involve

a neural network model that is trained with RSS input and the corresponding position labels. Replacing the entire localization process with a deep learning model causes problems regarding vulnerability to environmental changes, similarly to fingerprint-based methods. In this study, I propose a hybrid approach, which applies data-driven deep learning to only the ranging part of a model-based localization algorithm. By performing nonlinear regression using a neural network for the dual-band RSS, the ranging accuracy was significantly improved compared to that of the rule-based method. In addition, the proposed localization method has the advantage of being robust against changes in the AP locations and spatial structure. A ray-tracing method was used to get the channel data for a complex NLOS environment, and the ranging performance of the proposed dual-band RSS was evaluated and compared to that of existing methods. A comparison with existing methods using single-band RSS or rule-based ranging showed the advantages of the proposed method in terms of positioning accuracy. In addition, changes in the neural network structure of the deep regression model were analyzed.

The remainder of this paper is organized as follows. In the next section, I introduce some related studies. Section 3 explains the background of the propagation characteristics of electromagnetic waves indoors. Section 4 presents the system model and the proposed hybrid localization method using dual-band RSS. Section 5 presents a performance analysis of the proposed method compared to existing methods, and Section 6 outlines the conclusions of the study.

2.2 Preliminary

A free-space PLM can be represented based on the Friis transmission formula [44].

$$\mathrm{PL_{fs}} = 20\log_{10}(d) + 20\log_{10}(f) + 20\log_{10}(\frac{4\pi}{c}) - G_{\mathrm{Tx}} - G_{\mathrm{Rx}}, \qquad (2.1)$$

where $\mathrm{PL_{fs}}$ denotes the free-space loss on the decibel scale, d is the distance (m) between the transmitter and receiver, c is the speed of light, f is the frequency, and G_{Tx}

and G_{Rx} are the antenna gains of the transmitter and receiver, respectively. The PLM in a typical LOS environment is similar to that in free space, and the path-loss difference between the 2.4 and 5.2 GHz bands only has an offset according to the antenna gain and the frequency difference. However, in an NLOS environment, the PLM becomes more complicated. The site-general models are presented in previous research for indoor environments, [21–23]. Among them, I consider the IEEE 802.11 specification [21], which suggest a 2-slope model for the indoor Wi-Fi systems. The general model can be represented as shown in (2.2).

$$r(d) = \begin{cases} r(d_0) - 10\eta_0 \cdot \log_{10} \frac{d}{d_0} + X_0, \text{ if } d \leq d_{\mathrm{BP}} \\ r(d_{BP}) - 10\eta_1 \cdot \log_{10}(d - d_{BP}) + X_1, \text{ if } d > d_{\mathrm{BP}}, \end{cases} \tag{2.2}$$

where $r(d)$ is the RSS at distance d, and $r(d_0)$ is the RSS at the reference distance d_0. d_{BP} is the break-point distance, which divides two regions according to the distance from the transmitter. The two regions are modeled using different path-loss exponents, which are denoted by η_0 and η_1, and different shadowing factors, which are denoted by X_0 and X_1, respectively. This model is not appropriate for positioning, as it is a statistical model for analyzing the quality of service in general indoor environments. When radio waves propagate in a space with obstacles, they are affected by various phenomena, such as reflection, scattering, and diffraction. As a result, the path loss in an NLOS environment becomes extremely complex, and the average attenuation depends on the material of the obstacle and the radio wave frequency. For example, a cement wall, which is the most popular type of wall, shows significant differences in transmission and reflection properties for the 2.4 and 5.2 GHz frequencies [24]. Considering the influence of walls, Obeidat et al. [25] presented the following effective wall loss model, which is consistent with practical indoor environments:

$$r(d) = r(d_0) - 10\eta_f \cdot \log_{10}(\frac{d}{d_0}) - \Sigma_{v=1}^{V} W_v, \tag{2.3}$$

where η_f is the path-loss exponent, and W_v is the attenuation caused by the v-th wall in the propagation path. Focusing on the fact that the wall attenuation differs for each

frequency band, the NLOS mode can be estimated. Fig. 2.1 conceptually represents the attenuation tendency of the walls for two frequency bands. In free space, the attenuation in two bands is similar, but the difference in attenuation between two bands increases as there are more obstacles since the attenuation in 5.2 GHz is larger than that in 2.4 GHz for obstacles. In fig 2.1, the path loss is expressed according to the number of walls as if the discrete steps are clearly separated; however, in a practical environment, this is not clear because the attenuation varies depending on the wall thickness, material, and map composition. The key point is that the attenuation in the 5.2 GHz band for the same geometric environment tends to be large at a certain rate compared to that in the 2.4 GHz band, and this can be an indicator of the severity of the NLOS condition. I assume that there is a nonlinear relation between the severity of the NLOS condition and the difference in attenuation between two bands.

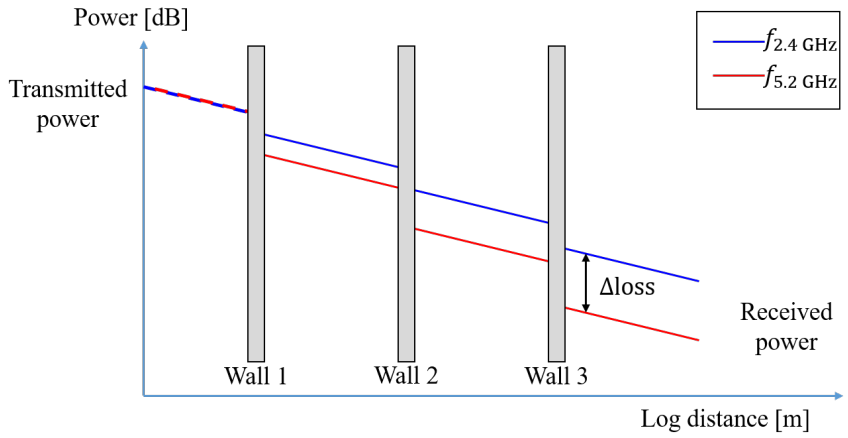

Figure 2.1: Indoor path loss for the different frequency bands.

2.3 System model

In this study, I assumed a Wi-Fi communication environment that uses a dual-band frequency. As shown in fig 2.2, when the RSS at the target point $\mathbf{x} = [x, y]^{\mathrm{T}}$ is measured by three or more APs, the RSS of the i-th AP is represented as $\mathbf{r}_i = [r_i^{2.4}, r_i^{5.2}]$, where $r_i^{2.4}$ and $r_i^{5.2}$ denote the RSS of 2.4 GHz and that of 5.2 GHz, respectively.

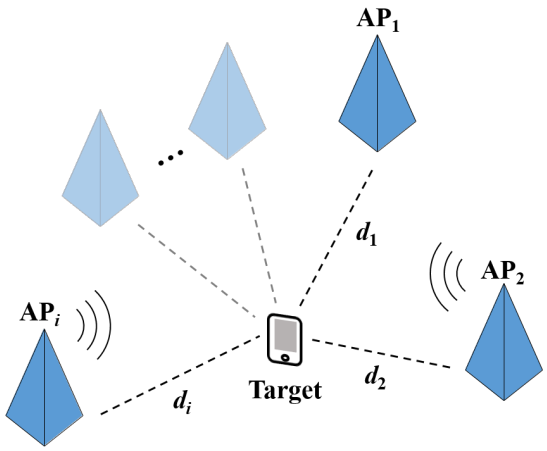

Figure 2.2: Range-based localization scenario.

The proposed hybrid localization scheme is illustrated in fig 2.3. The basic structure is the same as that of the typical range-based localization method. The distances between APs and target devices are estimated based on the RSS measured at the ranging stage, and the position of the target node is estimated using the n-distance estimates of n AP locations. In the ranging stage, the conventional rule-based method estimates the distance by using the inversion of the PLM, which represents the RSS attenuation according to the distance. For example, using the PLM in (2.2), the distance estimate $\hat{d}$ for the RSS value r can be calculated as follows.

$$\hat{d}(r) = \begin{cases} d_0 \cdot 10^{\frac{r(d_0)-r}{10\eta_0}}, & \text{if } r \leq r(d_{\mathrm{BP}}) \\ d_{\mathrm{BP}} + 10^{\frac{r(d_{\mathrm{BP}})-r}{10\eta_1}}, & \text{otherwise.} \end{cases} \tag{2.4}$$

In this study, I replaced this ranging part with a regression model that used deep

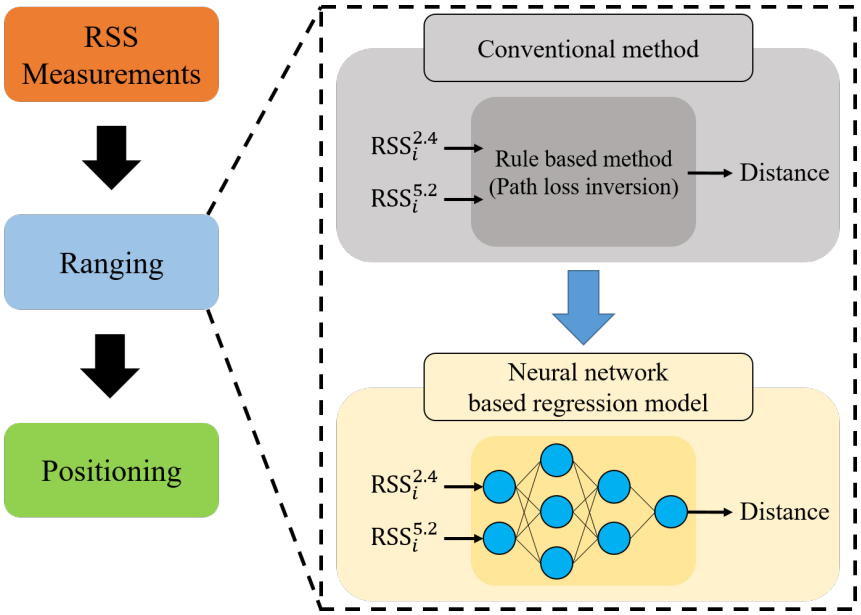

Figure 2.3: Proposed hybrid range-based localization scheme.

neural networks. The details of the proposed method of using a neural network are explained in the next section. After the distances from each AP are estimated, the positions of the target nodes are specified in the positioning stage. By using the known positions of the fixed APs and the estimated distances, trilateration-based algorithms can be applied. Among the various trilateration-based algorithms, the iterative least-square (ILS) method estimates the target position to be close to the optimal solution [45, 46]. The position estimate using ILS can be expressed as follows:

$$\hat{\mathbf{x}}^{(k)} = \begin{bmatrix} \widehat{x}^{(k)} \\ \widehat{y}^{(k)} \end{bmatrix} = \hat{\mathbf{x}}^{(k-1)} + \begin{bmatrix} \delta x \\ \delta y \end{bmatrix}, \tag{2.5}$$

where

$$\begin{bmatrix} \delta x \\ \delta y \end{bmatrix} = \begin{bmatrix} \frac{(x_1 - \widehat{x}^{(k-1)})}{d_1^{(k-1)}} & \frac{(y_1 - \widehat{y}^{(k-1)})}{d_1^{(k-1)}} \\ \vdots & \vdots \\ \frac{(x_N - \widehat{x}^{(k-1)})}{d_N^{(k-1)}} & \frac{(y_N - \widehat{y}^{(k-1)})}{d_N^{(k-1)}} \end{bmatrix}^{+} \begin{bmatrix} \widehat{d}_1 - d_1^{(k-1)} \\ \vdots \\ \widehat{d}_N - d_N^{(k-1)} \end{bmatrix}, \tag{2.6}$$

and

$$d_i^{(k-1)} = \sqrt{(x_i - x^{(k-1)})^2 + (y_i - y^{(k-1)})^2}, \tag{2.7}$$

where, $\hat{\mathbf{x}}^{(k)}$ is the position estimate for the k-th iteration, and (x_i, y_i) is the position of the i-th AP. The initial position estimate $\hat{\mathbf{x}}^{(0)}$ can be set as the center of the map. The proposed scheme is a hybrid method that is similar to the existing rule-based method, but only the ranging part was replaced with the data-driven deep learning method. The risk of overfitting was minimized by the data-driven learning part. Ultimately, the position accuracy is increased by improving the ranging accuracy.

2.4 Proposed Ranging Method

In this study, I propose a deep regression model for dual-band RSS ranging. The model's structure is shown in fig 2.4. The input of the model is the dual-band RSS vector, $\mathbf{r}_i$. The model has several hidden blocks, each of which is composed of a fully connected (FC) layer, a batch normalization layer, and a rectified linear unit (ReLU) activation function. The FC layer is a structure in which one node is connected to all other nodes in the adjacent layer. It allows for nonlinear regression along with a nonlinear activation function. Although the FC layer is simple and powerful, it is vulnerable to overfitting.To solve this problem, a batch normalization layer was inserted into each hidden block. The use of the batch normalization layer mitigates internal covariate shift phenomenon, which is the changes in the input data distribution affect the training procedure. Typically, batch normalization makes the neural network more stable and prevents the overfitting problem and increases the learning efficiency [47].

When the number of nodes of the FC layer of the l-th hidden block is $M^{(l)}$, an input is represented as $\mathbf{a}_l = [a_1, \ldots, a_{M^{(l)}}]^{\mathrm{T}}$, and the output of the FC layer is expressed as

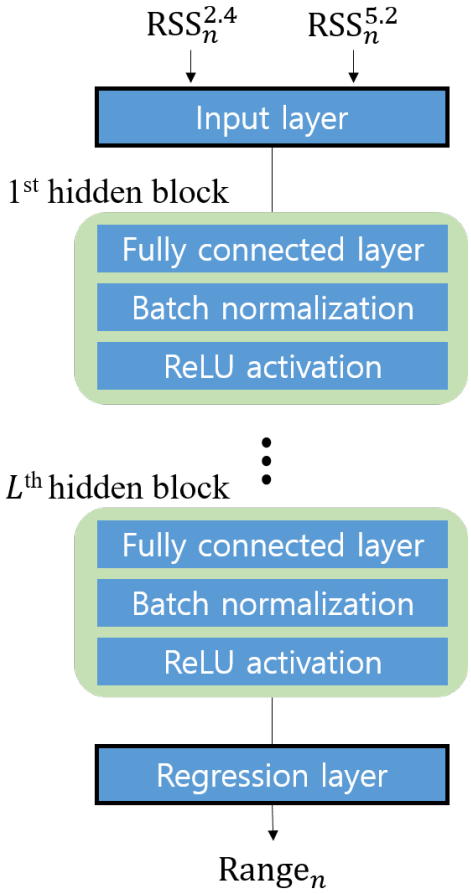

Figure 2.4: Neural network structure for deep regression.

follows:

$$\mathbf{y}^{(l)} = \begin{bmatrix} y_1^{(l)} \\ \vdots \\ y_M^{(l)} \end{bmatrix} = \mathbf{W}_l \cdot \mathbf{a}_l + \mathbf{b}_l, \tag{2.8}$$

where $\mathbf{W}_l$ is an $M^{(l-1)} \times M^{(l)}$ matrix representing the weights of the nodes in the FC layer, and $\mathbf{b}_l$ is a vector representing biases. These are parameters that can be trained using data-driven learning. With the mini-batch size K_B, the batch normalization result $\bar{y}_m^{(l)}$ for the j-th sample is expressed as follows:

$$\bar{y}_m^{(l)} = \gamma_m^{(l)} \cdot \left(\frac{y_{m,j}^{(l)} - \mu_{m,\mathrm{B}}}{\sqrt{\sigma_{m,\mathrm{B}}^2 + \epsilon}} \right) + \beta_m^{(l)}, \tag{2.9}$$

where $j \in [1, K_B]$, $y_{m,j}^{(l)}$ is the m-th node of the FC layer in the l-th hidden block. μ_{B} and σ_{B}^2 denote the sample mean and sample variance of $y_m^{(l)}$ in the mini-batch, respectively. The parameters $\gamma_m^{(l)}$ and $\beta_m^{(l)}$ are the scaling factors and shift factors, respectively, and these are also updated through the learning process. By re-centering and re-scaling the data for each layer, after batch normalization, the ReLU activation function is applied. The use of ReLU activation function mitigates the gradient vanishing problem that may occur in the FC layer, and allows the neural network with deep structure to be trained efficiently [48]. After the ReLU activation, the output of the l-th hidden block is as follows:

$$o_m^{(l)} = \begin{cases} 0, & \text{if } \bar{y}_m^{(l)} < 0 \\ \bar{y}_m^{(l)}, & \text{otherwise} \end{cases} \tag{2.10}$$

The regression layer after the total of L hidden blocks is the FC layer with one node, which performs the linear combination of the L-th hidden block's output. The proposed regression model can be trained with supervised learning by using the dual-band RSS vector and the ground truth distance value as a label. Let the ground truth distance be d_i, which corresponds to the i-th RSS vector; then, the mean square error (MSE) E with the model output can be expressed as follows:

$$E = \sqrt{(y_i - d_{\mathrm{i}})^2}. \tag{2.11}$$

To train the proposed model, the gradient of the MSE in (2.11) with respect to each parameter is computed by using the back-propagation algorithm, and the parameters of the model are updated to minimize the average MSE for the training dataset.

The overall process of the proposed localization method is summarized in Algorithm 1.

The number of hidden blocks and the number of hidden nodes constituting the proposed model are user-defined hyperparameters. The deeper the neural network is, the more complex the nonlinear function will be. However, there is a performance limit when the structure is excessively complex compared to the input data. In the next section, an analysis of the performance depending on the hyperparameters is presented.

2.5 Performance Evaluation

2.5.1 Ray-Tracing-Based Simulation

The proposed scheme assumes the installation of APs and the use of two frequency bands in an indoor environment. For the simulation, a geometry-based channel was created by using a ray-tracing method with real spatial information [49, 50]. Three sites with different materials and structures were investigated. Fig 2.5 represents the 3D views and floor plans of the three sites, where (a) and (b) are academic buildings (INMC and ASRI on the Seoul National University campus), and (c) is an apartment building. The locations of the APs on each floor plan are marked with red circles. The height of the APs was set to 1.5 m for each map. The Tx power was assumed to be 0 dBm, and the center frequency was set to 2.4 or 5.2 GHz.

Fig. 2.6 and fig.2.7 represent the RSS distribution according to the center frequency when only one specific AP is considered in the map shown in fig 2.5a. Similarly to the theoretical inference, the attenuation in the 5.2 GHz band is larger than that in the

Algorithm 1 Proposed localization procedure.

<**Offline stage**>

Input

Training set $\mathbf{R}'$: The set of dual-band RSS vector, $\mathbf{r}_i = [r_i^{2.4}, r_i^{5.2}]$,

and ground truth distance d_i for each sample

Validation set $\mathbf{V}'$: The set of validation data, which are same kind of data as,

but not included in the training set

Initialize a neural network described in fig 2.4 with random weights, biases, and normalization parameters.

for all training data grouped by mini-batch size of K_B, **do**

Forward calculation for the NN

The output y_i is a result of the last layer of the NN

Calculate the average MSE between y_i and d_i in the mini-batch

Update parameters of the NN, by using back–propagation

end for

Find best–fit parameters of the NN that minimize MSE for the validation set

Output Trained NN as a deep regression model

<**Online stage**>

Input

Test data location of N APs and N RSS vector

Set a confidence threshold Th_c

for each i-th AP **do**

Predict $\widehat{d_i}$ using the trained NN

end for

Find target position $\hat{\mathbf{x}}$, using Equation (2.5)–(2.7)

Output : Position estimate of target device $\hat{\mathbf{x}} = [\hat{x}, \hat{y}]^{\mathrm{T}}$

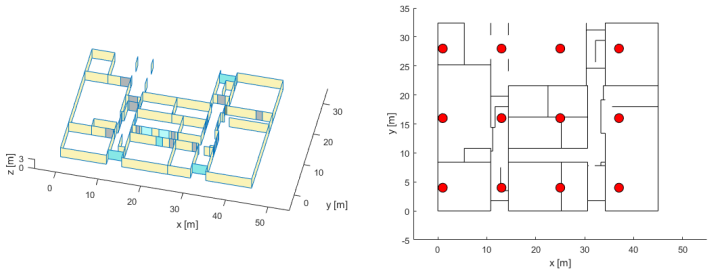

(a)

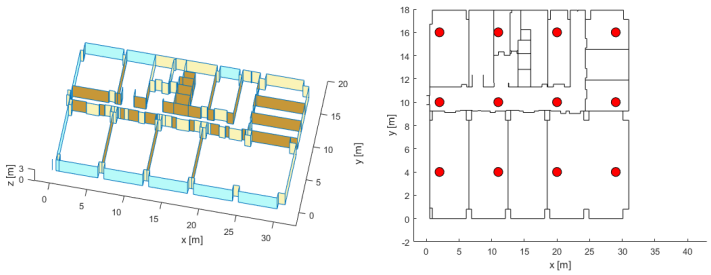

(b)

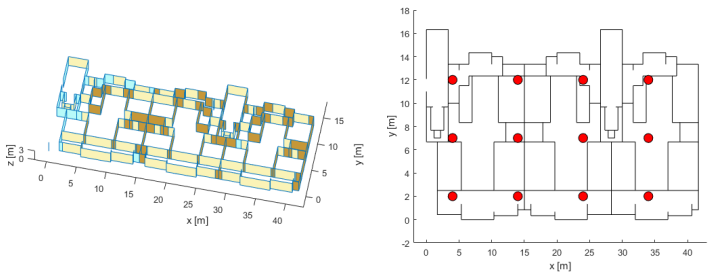

(c)

Figure 2.5: The 3D maps and the top views of the environments: (**a**) INMC (academic building), (**b**) ASRI (academic building), and (**c**) APT (residential space).

2.4 GHz band, and the difference in attenuation between the two frequency bands is verified to be larger under harsh NLOS conditions. For the evaluation of the ranging and positioning performance, the RSS values from 12 APs were recorded at points on a uniform grid approximately 1 m apart from each other for the three sites. The total number of points evaluated for the three sites was 11,474, and the number of RSS–distance pairs satisfying the noise floor condition was 74,912. All measurement points were split into sets with the following proportions: 70% for the training set, 15% for the validation set, and 15% for the test set; then, the deep regression model was trained and evaluated by using the dual-band RSS and distance pairs.

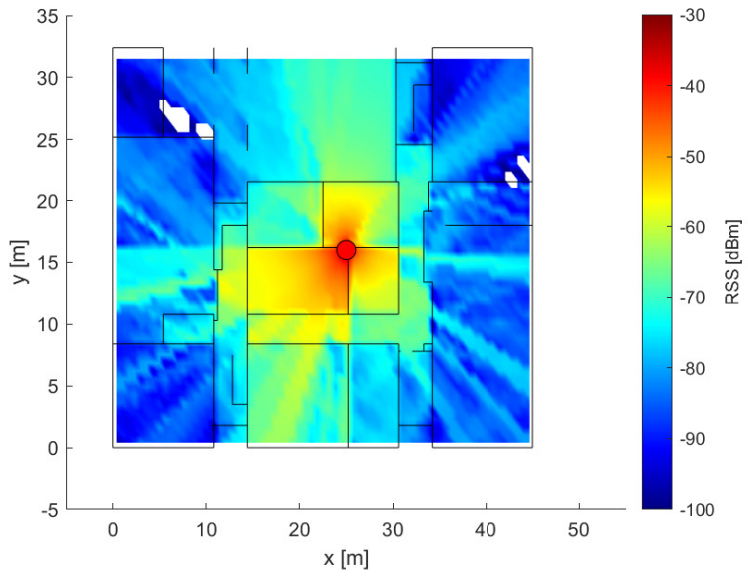

Figure 2.6: RSS map for an AP in the 2.4 GHz band.

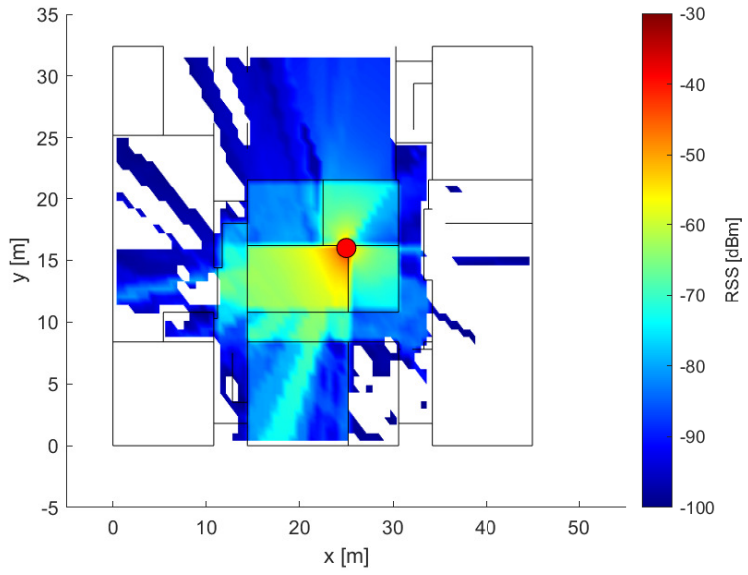

Figure 2.7: RSS map for an AP in the 5.2 GHz band.

2.5.2 Analysis of the Ranging Accuracy

Several existing ranging methods were used as benchmarks to verify the effectiveness of the proposed method. Most previous RSS based ranging method used a single-band RSS, To analyze the effect of using dual-band RSS, benchmarks 1 and 2 were set as a rule-based raging method using only RSS in the 2.4 and 5.2 GHz bands, respectively. These were based on a two-slope PLM as described in (2.2) that has been widely used in existing studies. The PLM parameters for each frequency band were optimized with linear regression to best fit the training data. For a single RSS measurement, the distance can be estimated by PLM inversion as presented in (2.4). The ranging accuracy of these methods can be affected by the accuracy of the PLM models. To consider more complex PLM, benchmarks 4 and 5 used a non-linear regression model using a neural network for single-band RSS data. Similar to the proposed method, deep regression models were learned using the only RSS in the 2.4 and 5.2 GHz bands. The benchmark 3 is the result of an existing rule-based ranging algorithm that uses the dual-band RSS described in [31]. In the ranging method of Benchmark 3, the channel states were divided into LOS, NLOS, and severe NLOS, and the path-loss exponents were different for each state. The parameters of this rule-based methods were also optimized to best fit the training data.

In fig 2.8, the results of benchmarks 1 and 2, which use the regression methods based on the two-slope PLM, are represented by black lines, and the regression model based on the neural network is expressed in green lines. The results in fig 2.8b,c show the limitations of the ranging method using a single-band RSS. As only one distance is mapped to one RSS value, the NLOS conditions cannot be distinguished. The regression results of the two-slope PLM and the results of the neural network are similar when using the single-band RSS. The ranging method using a neural network shows an improvement in ranging accuracy. However, there is an upper limit for the ranging method using the single-band RSS, regardless of how detailed the tuning applied is. Fig 2.8d shows the ranging results of the existing rule-based ranging method using

the dual-band RSS. In this method, two or more distances may correspond to the RSS value of one band. The distance can be estimated by classifying the NLOS conditions, but reflecting all of the various cases shown in (a) is difficult. In addition, because only the path-loss exponent is adjusted to estimate the distance for the NLOS conditions, there is a risk of amplifying the ranging error for misclassified cases.

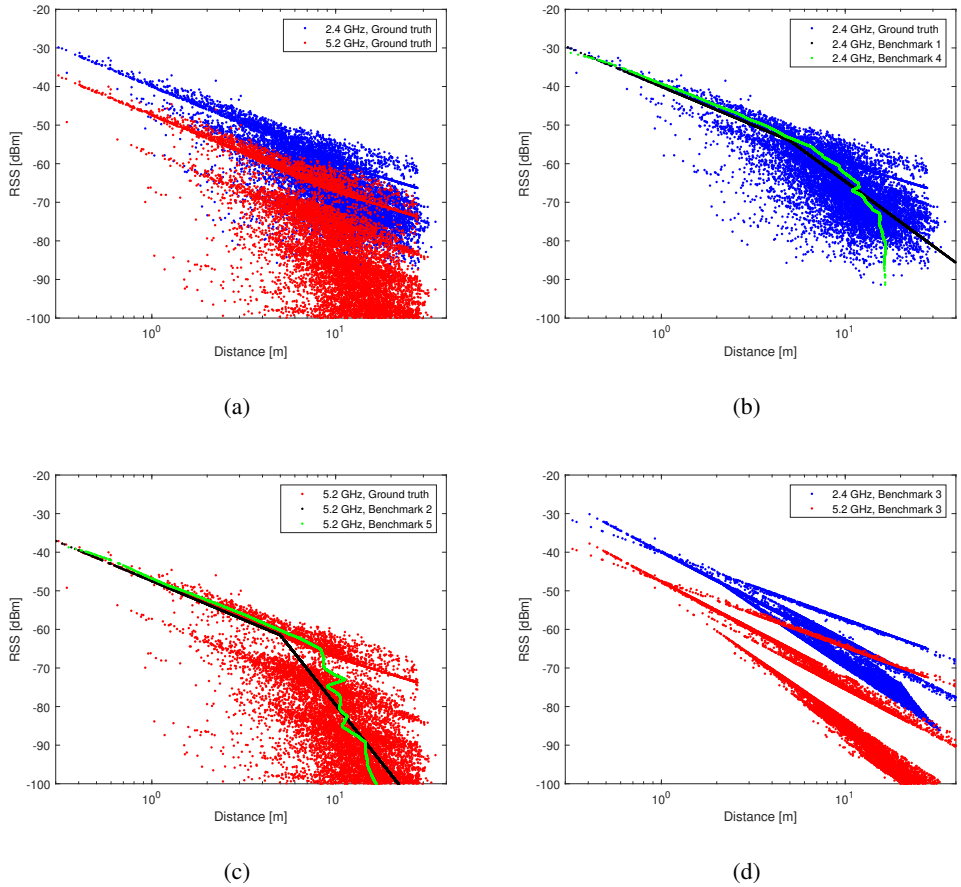

Figure 2.8: (**a**) Distance data of the ground truth, and the regression results of the (**b**) 2.4 GHz, (**c**) 5.2 GHz, and (**d**) dual-band frequencies.

The regression results of the proposed model are shown in fig 2.9. The NLOS conditions were divided into several stages by using the dual-band RSS input. This reflects the severe NLOS conditions, especially when there are multiple walls between anten-

nas. The deep regression model was trained using data from various cases. Therefore, it describes the ground truth of the test data better than the other rule-based models. In the performance evaluation, the number of nodes in the hidden block was set to 64, and the number of hidden blocks was set to 10.

Fig 2.10 shows the empirical cumulative distribution function (ECDF) of the ranging errors according to the ranging methods. The key indicators of the results are summarized in Table 2.1. In terms of the error between the estimated distance and the actual distance, the proposed method showed the best performance with a median error of 1.49 m. This is approximately 36.1% lower than those of the benchmark techniques. The benchmark results using the single-band RSS showed similar performances. This is because there is a limit to the information that can be obtained from the single-band RSS. The results of Benchmark 3, which used dual-band RSS, did not show good ranging accuracy for the test environment. This is due to the limitation of the rule-based ranging method in that it is difficult to reflect various cases in an indoor environment with only three discrete channel states. Although the ranging accuracy improved in some cases, the statistical performance of the total test samples was degraded because ranging errors were amplified by misclassification in several other cases.

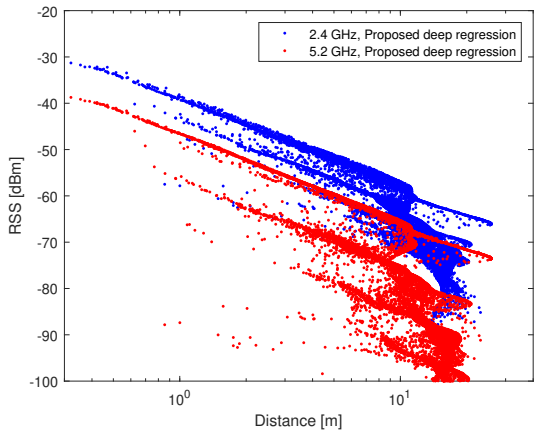

Figure 2.9: Regression results of the distance–RSS data with the proposed method.

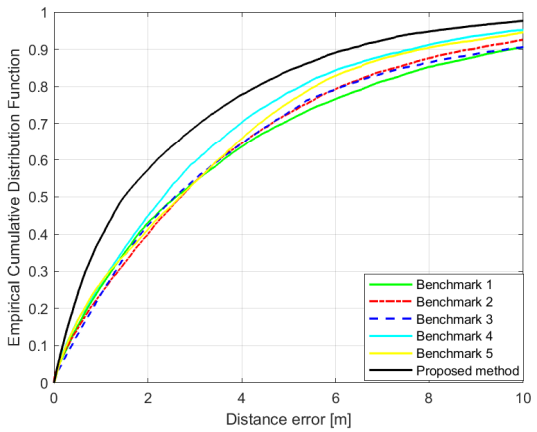

Figure 2.10: Empirical cumulative distribution function (ECDF) of the ranging error.

Table 2.1: Ranging error results of each ranging method

Ranging Method	**Ranging Error [m]**			
	25%-tile	**50%-tile**	**90%-tile**	**Average**
Benchmark1	0.96	2.60	9.75	4.05
Benchmark2	1.06	2.71	8.92	3.78
Benchmark3	1.05	2.57	9.67	4.580
Benchmark4	0.903	2.33	7.65	3.23
Benchmark5	0.88	2.68	7.85	3.471
Proposed method	0.53	1.49	6.28	2.52

2.5.3 Analysis of the Neural Network Structure

The hyperparameters of the proposed deep regression model are adjustable variables. There is a trade-off between the performance and computational complexity of the neural network. I evaluated the average value of the ranging error by changing the number of nodes and the number of hidden blocks, and fig 2.11 shows the results. The ranging error is saturated to about 2.5 m, and having too many hidden blocks for the small number of nodes decreases the ranging accuracy. The computational complexity of the proposed model structure can be expressed as $O(M^2 * L)$. Therefore, as the structure becomes more complex, the computation increases excessively compared to the performance gain. In this paper, I propose the use of 64 nodes in each layer and eight hidden blocks, where the ranging accuracy is greater than the 95th percentile value among the evaluated models, and the computational complexity is only 3.3% compared to the model with the highest ranging accuracy.

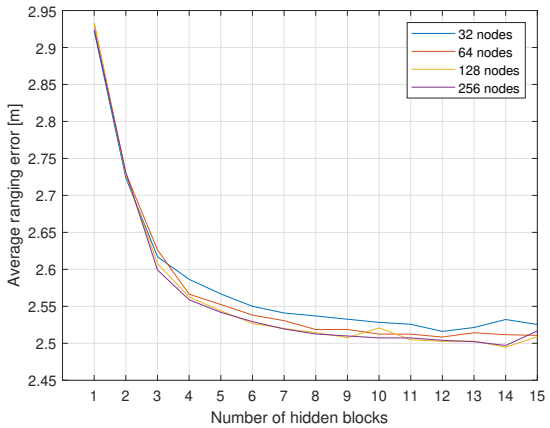

Figure 2.11: Average ranging error according to the structure of the neural network.

2.5.4 Analysis of Positioning Accuracy

To analyze the effect of our proposed ranging technique on the range-based localization accuracy, I used the ILS positioning method discussed in Section 2.2. In particular, to reflect a change in the channel environment, I assumed a change in the AP deployment, as shown in fig 2.12. The fingerprint-based methods cannot be applied without a new site survey, and the robustness of the proposed hybrid localization can be verified in this scenario.

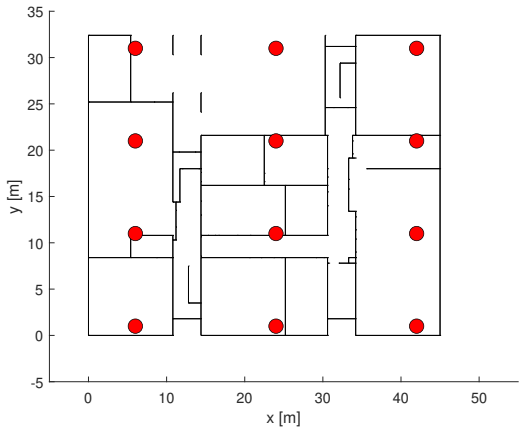

Figure 2.12: A top view of the test environment.

Fig 2.13a shows the ECDF of the root mean square error (RMSE) between the estimated and actual positions for a total of 1641 points. The key indicators are summarized in Table 2.2. In terms of statistical results, the performance of the proposed method was superior to that of the existing methods. The average RMSE of the proposed method is similar to that of Benchmark 1 due to the outlier result of the ILS positioning method. When comparing the median RMSEs, our proposed positioning method showed a lower error than those of other existing methods by at least 22.3%. Positioning results using the single-band RSS of 2.4 or 5.2 GHz had median errors of 2.73 m and 3.03 m, respectively, even when the deep regression method was applied. These are 3.8% and 9% smaller errors, compared to the results of using 2-slope PLM-

based method for each band. Meanwhile, the result of benchmarks 3, which was the result of the existing rule-based method using the dual-band RSS, was 2.56 m. Additionally, the deep regression ranging method using the dual-band RSS could reduce the median of positioning error to 1.99 m. It was a 22.3% improved result compared to the result of benchmark 3. The effect of the deep regression method was more significant with the dual-band RSS than with the single-band RSS.

Our proposed method is more effective for errors of the 50th percentile or less. The histogram in fig 2.13b shows the distribution of spatial positioning errors. In each histogram, the x-axis represents positioning RMSE, and the y-axis represents count. The result shows that proposed method improved the overall positioning accuracy, and increases the number of cases estimated within 2 m. This is because the proposed algorithm effectively reduces the ranging error when the AP and the target device are actually close to each other, but are blocked by walls.

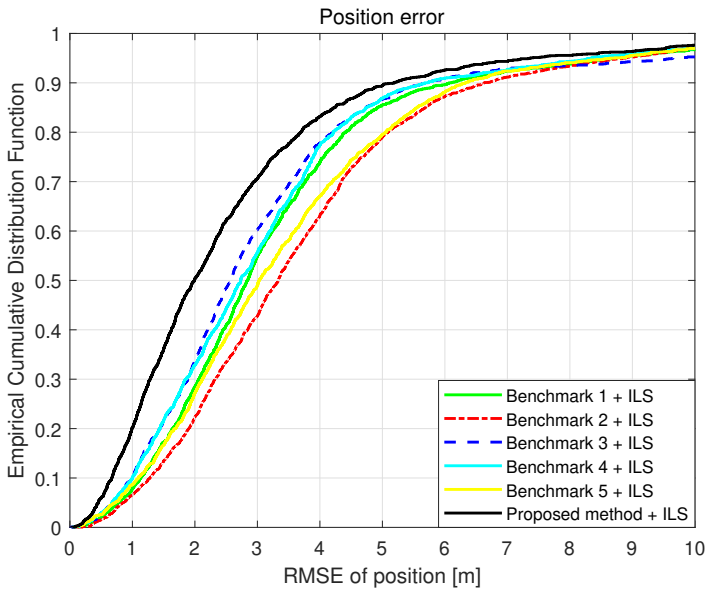

(a)

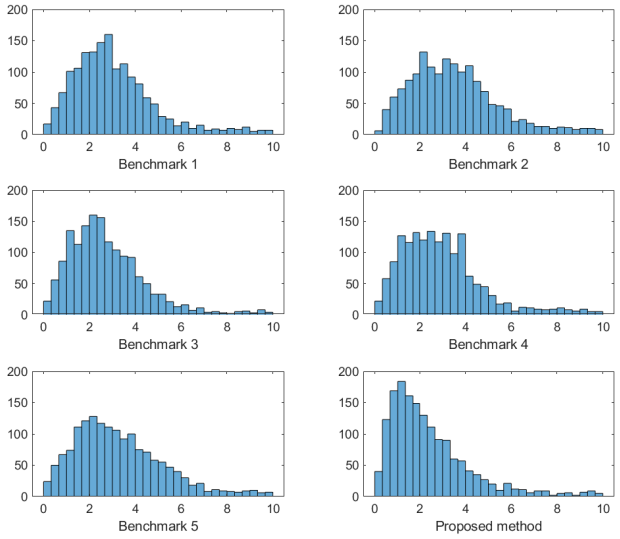

(b)

Figure 2.13: Empirical cumulative distribution function (**a**) and histogram (**b**) of the positioning error.

Table 2.2: Positioning error results for each ranging method

Ranging Method	**Positioning Error [m]**			
	25%-tile	**50%-tile**	**90%-tile**	**Average**
Benchmark1	1.85	2.84	6.09	3.82
Benchmark2	2.11	3.33	6.63	4.98
Benchmark3	1.66	2.56	5.69	11.38
Benchmark4	1.67	2.73	5.70	28.38
Benchmark5	1.93	3.03	6.33	4.82
Proposed method	1.14	1.99	5.19	3.68

2.6 Summary

In this study, I proposed a hybrid localization algorithm that replaces only the ranging part of the existing range-based localization method with a deep regression model that uses data-driven learning. For the ranging part, the accuracy of distance estimation in an indoor NLOS environment is improved by using the dual-band RSS, and this is designed to cover various cases by using regression with a neural network. The improvements in the ranging and positioning accuracy of the proposed method were verified through a ray-tracing-based simulation for general indoor spaces. Furthermore, the proposed localization method is compatible with various situations, even when the indoor structure is changed. The prevailing fingerprint-based methods are cannot be applied in the situation I assumed where the deployment of APs are different compared to the offline stage.

Based on the results of ray-tracing based simulation, the use of dual-band RSS could reduce the median of positioning error up to 2.56 m, which was a 9.9% smaller error than the error obtained with the single-band RSS alone in the rule-based localization. By applying the deep regression method to the ranging part, the median error of 1.99 m was obtained, which was a 22.3% improved result compared to the rule-based

method. Considering that the use of deep regression with single-band RSS only caused 10% or less performance gain, the combination of the dual-band RSS and the deep regression method was effective in improving the accuracy of range-based localization using RSS.

The robustness of the proposed method encourages the use of RSS localization because it can reduce the intensity of the site survey process. In addition, the proposed method has the advantage that it can be implemented by using only the beacon signals from APs, without any special communication overhead. This will be useful for small IoT devices that are difficult to mount with multiple types of sensors or high cost network interface controller.

However, some future research should be followed to apply the proposed method in various situations. In this study, I considered the wall structure as a major factor of the complex indoor channel. In the real environment, there are many small obstacles that cannot be reflected in the ray-tracing based simulation, and the RSS fluctuations caused by the multi-path effect. In addition, analysis of more diverse materials and interior structures is required. After all, for a deep regression ranging model that operates robustly in various environments, as much experiments as possible are required to train and to validate the model.

Nevertheless, the proposed method is still promising in that a properly trained ranging model can be used even in an untrained environment. In practice, I expect to increase the learning efficiency by using a transfer learning technique that tunes the model trained through simulation with relatively small dataset from real experiments. Furthermore, extending the research to the triple-band-based ranging method is possible by utilizing 6 GHz band communication, which is expected to be supported in the Wi-Fi 6E standard.

Chapter 3

Genetic Algorithm for Path Loss Model Selection in Signal Strength Based Indoor Localization

3.1 Motivation

Recently, several studies have been conducted on indoor location-based services (LBS). LBS can be combined with various applications such as indoor guidance, resource management, security, and surveillance. For various LBS, indoor positioning or the so-called localization technique is a core technology. It is the one of the major internet of things (IoT) enabling techniques [1–3] and is also a key technology for 5G based applications [4]. Several studies based on wireless communications have been conducted to estimate locations in an indoor environment where hard to use global navigation satellite systems (GNSS) due to the blockage and the degradation of GNSS signals. Specifically, studies have been conducted using wireless local area network (WLAN) standard (known as Wi-Fi) [3, 6, 26, 27, 51–60]. Currently, most mobile devices support Wi-Fi, which can provide received signal strength (RSS) information between a device and access point (AP). Therefore, Wi-Fi RSS based localization method can be implemented without any additional investment in the off-the-shelf systems. Wi-Fi localization can be classified into range-free localization and range-based localization.

The former provides an approximate location using only connectivity with APs [61,62] or includes fingerprinting techniques [3, 6, 26, 51, 52, 58–60].

Wi-Fi fingerprinting methods are typically composed of two stages: offline and online. In the offline stage, the signal patterns are measured at several reference points in advance. In the online stage, the temporal signal pattern is compared with the existing database to estimate the position. Various types of information are used as components of the signal patterns. The pattern can be implemented by measuring the RSS from multiple APs [54, 55, 58, 59], time of arrival (TOA) based information [54], or channel state information (CSI) which is more low-level information than RSS [26, 27]. These methods commonly require considerable effort for reference data collection in the offline stage and are prone to becoming a very site-specific algorithm. In other words, it is difficult for these methods to perform consistently in areas where the wireless channel changes due to movement of internal structures or obstacles, or where site surveys are not sufficiently conducted. Furthermore, these methods may require an additional offline stage to cope with changes in the number or location of APs, furniture, and other minor changes in the environment.

Range-based localization consists of a ranging stage and positioning stage. In the ranging stage, the distance between the mobile node and APs is estimated. The position can be estimated using a trilateration or triangulation-based geometric method in the positioning stage [40, 45, 46, 56, 63–66]. Range-based localization is advantageous because it can be used in most commercial devices, and it does not require as much site survey as the fingerprinting methods. In the RSS ranging stage, the path loss model (PLM) inversion or a polynomial of the RSS can be used [38]. Most of these studies assume a 1-slope or 2-slope PLM similar to the one represented by the IEEE 802.11 standard [21]. When considering the path loss inversion method, the RSS ranging method needs an accurate PLM for indoor environments [39,67]. However, ranging errors are inevitable because it is very difficult to reflect the site-specific channel model in a real indoor environment. Among these errors, a distortion of the estimated distance

due to the non-line-of-sight (NLOS) condition is the most significant problem [38].

To mitigate ranging errors, it is necessary to determine the proper PLM for indoor localization. A few studies have aimed to improve the ranging performance by setting more suitable channel parameters, such as the path loss exponent (PLE) and an additional loss term [41, 42, 45, 68], or, by estimating the channel parameter directly in the locations where the APs are installed [40, 63, 69, 70]. In addition, in a recent study, a ranging technique was proposed where the channel characteristics are reflected in a neural network using an unsupervised learning process [54]. Methods for optimizing channel parameters require a large amount of measurement or pre-learning at the target locations. Furthermore, a model that is highly tuned to specific place risks loss of generality and is vulnerable to temporal and spatial changes in the site. Therefore, the channel model used for the ranging process should not be too general or too site-specific.In addition, it is necessary to consider that the channel characteristic between the mobile device and each AP can change in every localization trial due to the movement of people and objects. The previous studies assumed the same PLM for multiple APs, fluctuating the RSS value. However, to obtain an accurate ranging result from RSS value in indoor environments, it is indispensable to consider the coexistence of PLMs with different states for each AP.

This paper proposes an RSS-based localization method based on the overlapped multi-state PLM to reflect various channel characteristics for indoor environments. The overlapped multi-state PLM is formulated as if it were a superposition of potential 1-slope models, which can cover the channel states of all APs connected with a device at given instant in time. In the proposed method, distances between the mobile device and APs are estimated as several candidate values based on the overlapped multi-state PLM, combinations of estimated distances are calculated using trilateration, and the position is selected from these combinations by minimizing the residual error of localization. To reduce the complexity burden of finding the optimal channel combination, a genetic algorithm (GA) is applied. A detailed algorithm description and

analysis of the computational complexity are presented in later sections. The proposed method improves the accuracy of RSS-based indoor localization while minimizing site surveys and channel parameter tuning. I evaluated the localization performance of the proposed algorithm using a numerical analysis via ray-tracing based simulations for indoor environments and with experiments at a real site.

The contributions of this paper can be summarized as follows:

1) To cope with complex indoor channels, a method considering an overlapped multi-state PLM is proposed. This method can be used in general indoor places adaptively, without prior site investigation.

2) I design an efficient search algorithm using a GA to reduce excessive computation and enable practical usage while maintaining the positioning accuracy.

3) The proposed localization method only uses the RSS, which is available in most off-the-shelf products. Therefore, it can be implemented without additional hardware cost. Localization performance is verified with ray-tracing based simulations and real site experiments for Wi-Fi.

The remainder of this paper is organized as follows. In the next section, I present RSS-based ranging and positioning techniques. In Section III, I propose a localization method based on an overlapped multi-state PLM. Section IV shows a performance analysis of the proposed method through ray-tracing based simulations and real on-site experiments for Wi-Fi. Section V outlines the conclusions of the study.

3.2 Preliminary

I consider a range-based positioning scenario, where N APs and a device are located in a two-dimensional space as illustrated in Fig. 3.1. I denote $\mathbf{x} = [x, y]^{\mathrm{T}}$ and $\mathbf{x}_i = [x_i, y_i]^{\mathrm{T}}$ as the coordinates of the device and i-th AP, respectively. RSS information can be measured from both in device or APs. For example, the device can obtain

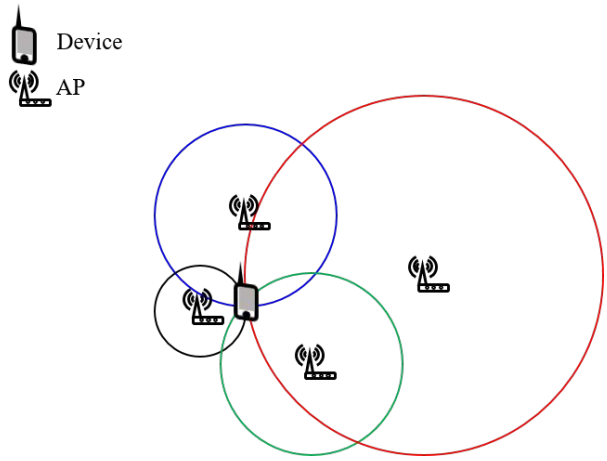

Figure 3.1: An example of RSS based localization.

RSS from all nearby APs by receiving the beacon frames transmitted by each AP. Conversely, APs can also measure RSS by detecting a packet of the device. I denote $\mathbf{r} = [r_1, r_2, ..., r_N]^{\mathrm{T}}$ as a vector of RSS measurement, where r_i represents the RSS from the i-th AP. Depending on the amount of signal attenuation, the distance from each AP can be estimated. Subsequently, the location of the device can be obtained by applying trilateration techniques with distance estimated from multiple nearby APs. In this section, I briefly summarize RSS-based ranging and positioning techniques.

3.2.1 RSS-based Ranging Techniques

The amount of signal attenuation from the transmitter can be explained by propagation model. 802.11TGn model provides an indoor channel model for typical Wi-Fi systems [21]. The main factors affecting the indoor distance estimation include the channel characteristic elements and attenuation based on the distance, corresponding to a large scale fading and shadowing effect due to walls or obstacles. The small scale fading effect due to a multi-path can be disregarded for RSS based ranging, as it causes small change in RSS compared to the aforementioned factors and can be mitigated by averaging RSS in a very short time [38, 71]. Thus, the attenuation for ranging can be

expressed with the PLM. The simplest PLM is a 1-slope model, which represents the RSS in decibel scale at distance d from the transmitter as

$$p(d) = p(d_0) - 10\eta \log_{10} \frac{d}{d_0} + X, \tag{3.1}$$

where $p(d_0)$ is the RSS at a reference distance d_0 and η is the PLE. In addition, X represents a shadowing factor, which is typically modeled as a zero mean Gaussian random variable with the standard deviation of σ.

To model sophisticated attenuation pattern more accurately, a 2-slope model is proposed [21]. This model predicts the RSS as

$$p(d) = \begin{cases} p(d_0) - 10\eta_0 \log_{10} \frac{d}{d_0} + X_0, \text{ if } d \leq d_{\text{BP}} \\ p(d_{BP}) - 10\eta_1 \log_{10}(d - d_{BP}) + X_1, \text{ if } d > d_{\text{BP}}, \end{cases} \tag{3.2}$$

where d_{BP} is called the break point distance, which separates two regions depending on the distance from the transmitter. The two regions are modeled using different PLEs denoted by η_0 and η_1, and different shadowing factors denoted by X_0 and X_1, respectively. In the indoor, the transition at d_{BP} is mainly because of the obstructions, and the points father than d_{BP} can be considered in NLOS condition [72]. The indoor path loss characteristic and the parameters have been studied much and the other standard documents also propose similar models by synthesizing the results of previous research [22, 23].

Using the one-slope PLM in (3.1), the distance from an AP can be estimated by

$$\hat{d}(p) = d_0 10^{\frac{p(d_0)-p}{10\eta}}, \tag{3.3}$$

where p represents the current RSS measurement from the AP. In case that the 2-slope PLM is used, I can estimate the distance depending on the RSS as follows:

$$\hat{d}(p) = \begin{cases} d_0 10^{\frac{p(d_0)-p}{10\eta_0}}, \text{ if } p \leq p(d_{\text{BP}}) \\ d_{\text{BP}} + 10^{\frac{p(d_{\text{BP}})-p}{10\eta_1}}, \text{ otherwise.} \end{cases} \tag{3.4}$$

Remark 1: The measured RSS is generally affected by various factors such as the distance between the AP and the device, presence of an obstacle, and antenna directionality. A dynamic shadowing effect caused by the walls, obstacles, and moving people, which makes accurate modeling difficult in practical indoor environments.

3.2.2 Positioning Technique

With distance estimates from at least three nearby APs, I can estimate the position of the device using trilateration methods. The estimated position $\hat{\mathbf{x}}$ can be expressed by

$$\hat{\mathbf{x}} = \arg\min_{\mathbf{x}} \epsilon(\mathbf{x}), \tag{3.5}$$

where $\epsilon(\mathbf{x})$ represents the cost function, which is defined as the square sum of ranging errors. It is represented by

$$\epsilon(\mathbf{x}) = \sum_{i=1}^{N} \Big(\|\mathbf{x} - \mathbf{x}_i\| - \hat{d}(p_i) \Big)^2, \tag{3.6}$$

where $\|\mathbf{a}\| = \sqrt{\mathbf{a}^{\mathrm{T}}\mathbf{a}}$ indicates the L2-norm of a column vector $\mathbf{a}$, and $\hat{d}_i$ represents the distance estimate from the i-th AP using either (3.3) or (3.4) depending on the PLM used for the ranging procedure. Two basic trilateration approaches can be found in literature: (i) the linear least square (LLS) method that computes $\hat{\mathbf{x}}$ using matrix operations [64], and (ii) the iterative least square (ILS) method that iteratively obtains the solution [45, 46].

In this work, we use the ILS method, which has been known to produce more precise positioning results than the LLS method [45]. The ILS method begins with a coarse estimate of the device's position. To this end, I simply initialize the device's position as the center of all nearby APs as follows:

$$\hat{\mathbf{x}}^{(0)} = \frac{1}{N} \sum_{i=1}^{N} \mathbf{x}_i. \tag{3.7}$$

At iteration $k \geq 1$, the ILS method updates the estimated coordinates of the device as

$$\hat{\mathbf{x}}^{(k)} = \hat{\mathbf{x}}^{(k-1)} - \lambda \frac{\partial \epsilon(\mathbf{x})}{\partial \mathbf{x}} \Big|_{\mathbf{x}=\hat{\mathbf{x}}^{(k-1)}}, \tag{3.8}$$

where $\hat{\mathbf{x}}^{(k)}$ represents the estimated position of the device after k iterations, and λ denotes the learning rate that controls the convergence speed. The derivative of the cost function with respect to $\mathbf{x}$ is derived as

$$\frac{\partial \epsilon(\mathbf{x})}{\partial \mathbf{x}} = \sum_{i=1}^{N} 2\left(\|\mathbf{x}-\mathbf{x}_i\| - \hat{d}_i\right) \frac{\mathbf{x}-\mathbf{x}_i}{\|\mathbf{x}-\mathbf{x}_i\|}. \tag{3.9}$$

The update process presented in (3.8) is executed until the solution converges. In most indoor localization scenario, the solution nearly converges in 10 iterations [46].

Remark 2: In existing localization methods, the factor that mainly causes the ranging error is the imperfection of the PLM. Ranging error usually causes a large residual error in the LS based methods and sometimes even makes the solution diverge in the ILS method. To prevent this, it is necessary to estimate the distance using a proper PLM. However, whether a fixed empirical model or a trained model is used, it is difficult to reflect channel characteristics that change with time and device location. At a certain instant in time, the channel from the mobile device to each AP may be different, and even for the same AP, the channel characteristics change due to movement of the device.

3.3 Proposed localization method

In this section, I define the overlapped multi-state PLM to improve ranging accuracy under dynamic indoor channel characteristics. Based on the overlapped multi-state PLM, a localization method is proposed. Then, a GA is applied to reduce the computational complexity of the proposed localization.

3.3.1 Localization Algorithm with Overlapped Multi-State Path Loss Model

Let us define K to be the number of states for the overlapped multi-state PLM and N as the number of APs. The k-th state for the overlapped multi-state PLM is defined as

$$p_k(d) = p(d_0) - 10\eta_k \log_{10}\frac{d}{d_0} - \beta_k + X_k, \tag{3.10}$$

where η_k is the PLE, X_k represents the shadowing term, and β_k denotes a constant offset for the k-th PLM. Even with the same RSS measurement from an AP, the distance from the AP can be estimated differently depending on the PLM. With the current RSS measurement p from an AP, the estimated distance using the k-th PLM is expressed by

$$\hat{d}_k(p) = d_0 10^{\frac{p(d_0)-\beta_k-p}{10\eta_k}}. \tag{3.11}$$

The overlapped multi-state PLM reflects various channel characteristics in practical indoor environments. By varying the PLM parameters η and β of each state, the proposed model can contain various channel situations. To consider indoor environment where LOS and NLOS states are mixed, K should be more than 2. In particular, to subdivide the NLOS state, I set K to be 4 or 8 herein.

The main differences between the conventional channel model in (3.2) and the proposed channel model in (3.10) are the number of states and the manner in which the PLM components constitute each channel model. In (3.2), two regions are classified according to the break point distance. Because (3.2) is a one to one function, it cannot accurately estimate the distances for all APs in complex situations, for example, RSSs are same, but distances are different or vice versa. However, in (3.10), I consider all possible PLMs for the same RSSs until the optimal combination of PLM states is selected. This is why the proposed model is termed as an "overlapped" multi-state pathloss model. Here, the discrete PLM parameter setting estimates the combination of channel states of APs using less information following the proposed algorithms.

For a given RSS measurement vector, K PLM states should be considered for each AP. To this end, I denote $s(i) \in \{1, ..., K\}$ as a specific choice of PLM state for the i-th AP and define a vector $\mathbf{s} = [s(1), ..., s(N)]^{\mathrm{T}}$ to represent the selection of the PLM for every AP. In addition, I denote $\mathcal{S}$ as the set of all possible combinations of $\mathbf{s}$, where the number of elements in this set is denoted by K^N as each AP can select one out of K PLM states.

Fig. 3.2 shows an example of localization based on overlapped multi-state PLM,

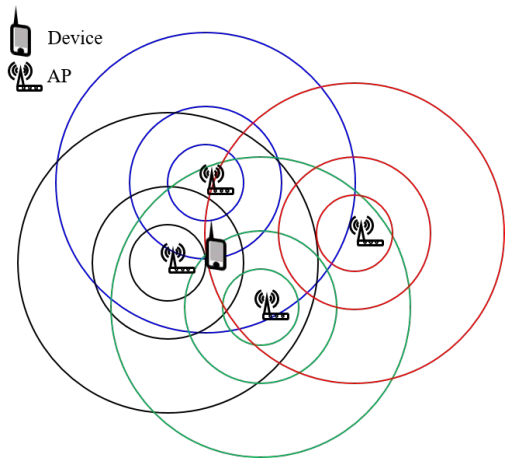

Figure 3.2: An example of positioning with multi state ranging.

where $K = 3$ and $N = 4$. Based on the overlapped multi-state PLM in (3.10), K distances are estimated for each AP. The assumption of overlapped multi-state PLM results in concentric trajectories centered on the AP. Hence,the circles intersect each other at several points in Fig. 3.2, and a combination of PLM states for each AP is equivalent to a combination of one circle per AP in Fig. 3.2. Using the ILS method, I can estimate the solution of $\mathbf{x}$ for each combination of PLM states $\mathbf{s} \in \mathcal{S}$.

Our objective is to determine the optimal combination of PLM states $\hat{\mathbf{s}}$ and position estimate $\hat{\mathbf{x}}$ at the same time, by minimizing the residual errors as

$$(\hat{\mathbf{x}}, \hat{\mathbf{s}}) = \underset{\mathbf{x},\mathbf{s}\in\mathcal{S}}{\arg\min}\, \bar{\epsilon}(\mathbf{x}, \mathbf{s}), \tag{3.12}$$

where the cost function is defined as

$$\bar{\epsilon}(\mathbf{x}, \mathbf{s}) = \sum_{i=1}^{N} \left(\|\mathbf{x} - \mathbf{x}_i\| - \hat{d}_{s(i)}(p_i) \right)^2. \tag{3.13}$$

The channel state of each AP cannot be found individually and can be determined by investigating the residual error from the overall combination. This makes the optimization problem in (3.12) be non-linear. Therefore, too much computational cost must be expended to find an optimal solution for this problem in a general way. Notably, K^N channel state combinations severely increase the amount of computation

required. The thorough searching method that calculates all cases in a search space is called as the exhaustive search or brute-force search. In addition to the process of finding a combination of channel states suitable for each AP, the exhaustive search algorithm eventually estimates the optimal location of the device under possible PLM combinations. A methodology using the residual error to select or calibrate channel parameters has been verified previously [54, 63]. The procedure of finding the optimal solution via exhaustive search is summarized in Algorithm 2. Although the optimal solution can be found with this method, the computational overhead is too large.

Algorithm 2 Exhaustive Search for Proposed Multi State PLM

Input: Position of N APs $\mathbf{x}_1, ..., \mathbf{x}_N$ and RSS vector $\mathbf{p} = [p_1, \ldots, p_N]^{\mathrm{T}}$

K : The number of possible state for each APs

N : The number of APs

for $\mathbf{s} \in \mathcal{S}$ **do**

  for i = 1 to N **do**

    Compute distance estimate $\hat{d}_{s(i)}(p_i)$

  end for

  Find an optimal position $\hat{\mathbf{x}}_{\mathbf{s}}$ using ILS method

  Calculate error $\bar{\epsilon}(\hat{\mathbf{x}}_{\mathbf{s}}, \mathbf{s})$ in (3.13)

end for

Select $\hat{\mathbf{s}}$ with the smallest $\bar{\epsilon}(\hat{\mathbf{x}}_{\mathbf{s}}, \mathbf{s})$ and denote $\hat{\mathbf{x}} = \hat{\mathbf{x}}_{\hat{\mathbf{s}}}$.

Output : Position estimate of target device $\hat{\mathbf{x}} = [\hat{x}, \hat{y}]^{\mathrm{T}}$

3.3.2 Localization with Genetic Algorithm-Based Search

To reduce the computational complexity of the Algorithm 2, I design a search method that applies a GA. The application of a GA in an optimization problem can increase

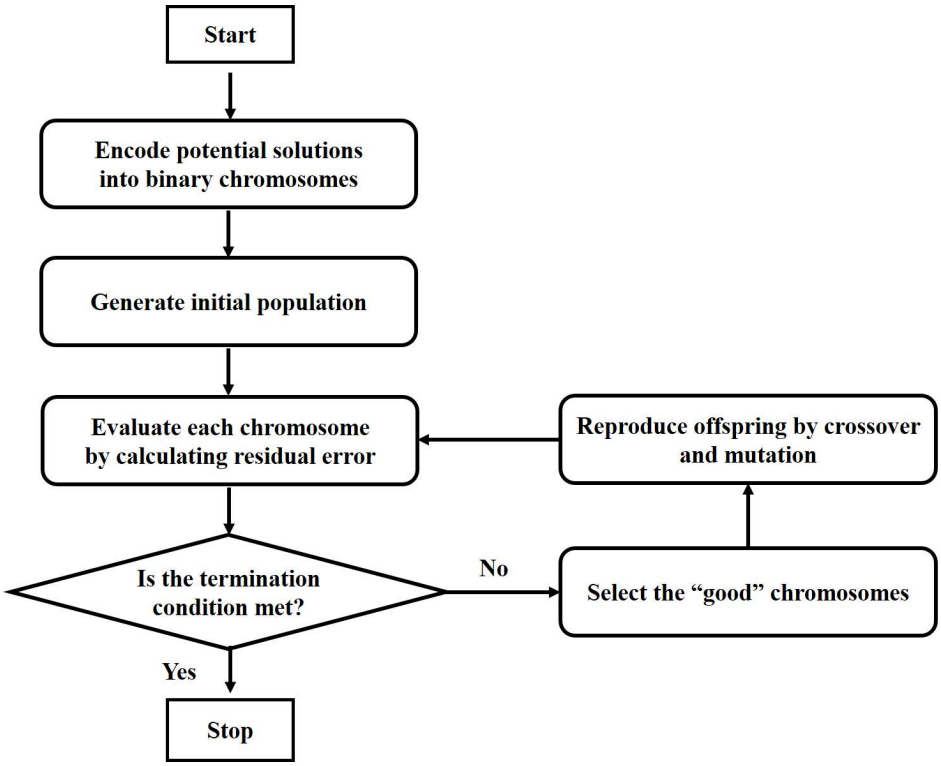

Figure 3.3: A block diagram of genetic algorithm.

efficiency greatly. It does not always guarantee a globally optimal solution, however it can find a sub-optimal solution within a reasonable amount of computation time [73]. Fig. 3.3 shows a block diagram of a typical GA. Based on this workflow, we developed the proposed positioning algorithm.

First, each of K PLM state is encoded in a form of gene, which is expressed by $\lceil \log_2 K \rceil$ bits. For instance, in case of $K = 8$, each PLM state is expressed by a gene from a set of 3 bit sequences $\{000, 001, ..., 111\}$. Using the encoded genes, the selection of PLM state for N AP can be expressed.

When an RSS vector is measured from N APs, the candidate solution, which is a combination of the potential channel models, can be expressed in the form of a $3N$ bit chromosome, $\mathbf{g} = [g(1), g(2), ..., g(N)]$. For instance, an arbitrary $\mathbf{s} = [1, 2, 7, 3]$ is encoded into $\mathbf{g} = [000\,001\,110\,010]$.

After the encoding stage, a population consisting of initial candidate solutions are randomly generated. The pool size of the initial population should be adjusted according to the size of the problem. For indoor localization, the number of APs and the number of potential PLMs should be considered. Once the pool size has been determined, a population set $\mathcal{G}$ is composed of $\mathbf{g}_n$ vectors initialized to arbitrary binary values, where n ranges from 1 to the pool size. It corresponds to a randomly selected subset in $\int$, and each chromosome $\mathbf{g}_n$ is a potential solution of a combination of PLM states for a given RSS vector.

Each candidate solution is ranked using the evaluation process. In this case, the residual error is calculated using a position estimation algorithm by assuming channel state combination corresponding to each chromosome. For evaluation and ranking, each chromosome $\mathbf{g} \in \mathcal{G}$ is decoded into channel state combination $\mathbf{s}$ and the residual error $\bar{\epsilon}(\hat{\mathbf{x}}, \hat{s})$ is calculated. Based on this, only 20% of the population is selected to remain in the order of small residual error. Let $\bar{\mathcal{G}}$ denote the selected 20% of the population in $\mathcal{G}$.

Then, child solutions are reproduced by crossovers from two randomly selected chromosomes in the selected group. The reproduction procedure mainly comprises two genetic operators: crossover and mutation. I applied a general method as presented in [73]. Two chromosomes are randomly picked in $\bar{\mathcal{G}}$ and mated. A random crossover point is selected and based on this, the tails of two chromosomes are swapped to generate child chromosomes as described in Fig. 3.4 (a). The figure shows a special case where chromosomes are 12 bits. In this way, the child population is reproduced up to the pool size. For the generated chromosomes, a mutation process is performed that converts all bits of solutions to opposite bits with a low probability (approximately 1-5% in this case). Fig. 3.4 (b) shows a conceptual example of the mutation operator. This process prevents the local minima problem, where the final solution is biased by the initial parent group. That is, even if the initial set randomly generated is somewhat wrong, the GA causes to near-optimal solution with high probability.

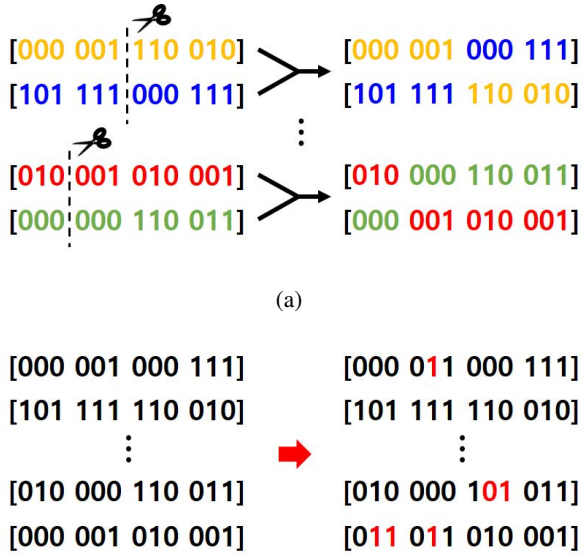

Figure 3.4: Example case of the genetic operator: (a) Crossover and (b) Mutation.

For the reproduced set $\mathcal{G}$, the evaluation and reproduction processes are repeated until the termination conditions are satisfied. In general, this iterative process can be terminated when the maximum iteration limit is reached, when the residual error of a specific solution satisfies the minimum criteria, or when there is no further improvement in the successive iteration. A pseudo code of the proposed method is summed up in Algorithm 3

Before the positioning process, the accuracy of the PLM states cannot be determined by observing the signal strength from one AP. When there are observations from multiple APs, the residual error of estimation is greatly reduced when the channel selection of each AP is inconsistent with each other. Due to these characteristics, solutions containing a subset of genes with consistency in the genetic search process are likely to survive in the evaluation and reproduction process. These subsets are merged to select a solution close to the optimal state. Through this process, the near-optimal solution is gradually obtained.

Algorithm 3 Proposed localization algorithm using multi-state overlapped PLM and GA based search

Input : Position of N APs $\mathbf{x}_1, ..., \mathbf{x}_N$ and RSS vector $\mathbf{p} = [p_1, \ldots, p_N]^{\mathrm{T}}$

m : The pool size of an generation

N : The Number of APs

(Initialization)

Encode PLM states into chromosomes with binary format

Generate a set of m initial population as $\mathcal{G} = \{\mathbf{g}_1, ..., \mathbf{g}_m\}$

while max iteration not reached or the best fitness $\leq$ threshold **do**

for $\mathbf{g} \in \mathcal{G}$ **do**

Recover PLM state vector $\mathbf{s}$ from $\mathbf{g}$

for i = 1 to N **do**

Compute distance estimate $\hat{d}_{s(i)}(p_i)$

end for

Find an optimal position $\hat{\mathbf{x}}_{\mathbf{s}}$ using ILS method

Calculate residual error $\bar{\epsilon}(\hat{\mathbf{x}}_{\mathbf{s}}, \mathbf{s})$ in (3.13)

end for

(Reproduction)

Rank results in order of low $\bar{\epsilon}$ and select top 20% as a parent set

Reproduce child chromosomes from the parent set, by using crossover and mutation operation

end while

Select the optimal state $\hat{\mathbf{s}}$ with the smallest $\bar{\epsilon}(\hat{\mathbf{x}}_{\mathbf{s}}, \mathbf{s})$ and denote the estimated position as $\hat{\mathbf{x}} = \hat{\mathbf{x}}_{\hat{\mathbf{s}}}$.

Output : Position estimate of target device $\hat{\mathbf{x}} = [\hat{x}, \hat{y}]^{\mathrm{T}}$

Near-optimal solutions from GA are not guaranteed to be global optimal. Nevertheless, it is advantageous to use GAs because of the computational benefit. Table 3.1 shows the relative computational complexity of the presented algorithms. When defining the computational complexity of the ILS method with conventional PLM as 1, the computational complexity with exhaustive search and K-state PLM is approximately K^N. As the number of APs (N) increases, the computational complexity becomes too high. On the contrary, the GA based search method can restrict computational complexity to a certain level. Even though there is a trade-off between the quality of the near-optimal solution and computational complexity, the proposed algorithm can be expected to find a good enough solution with the complexity restricted to below 2000. The numerical verification is discussed in the next section.

Table 3.1: Relative computational complexity

	ILS	Exhaustive search	GA based search
Conventional PLM	1	-	-
4-state PLM	-	4^N	~ 2000
8-state PLM	-	8^N	~ 2000

3.4 Performance evaluation

This section presents a performance analysis of the proposed localization methods using numerical simulations and experiments in indoor environments. For numerical simulations, RSS data are generated using 3-dimensional ray-tracing technique as described in [50], which utilize the spatial information of real sites. In the ray-tracing simulation, the power of each path between antennas is calculated using the wall information, considering propagation, reflection, and transmission loss. By synthesizing the calculated ray information, it is possible to simulate the RSS attenuation characteristics similar to the real measurement. Experimental measurements are also per-

formed using commercial smartphones and APs in indoor environments. Especially, I conducted measurement in an emergency room in a hospital, where the localization technology is required for resource monitoring or surveillance. As a benchmark to verify the effectiveness of the proposed overlapped multi-state pathloss model, we set the conventional PLM as a single state PLM composed of 2 slopes depending on the distance, like in [21]. In this model, d_{BP} and reference power are user defined factors. I set d_{BP} as 5 m, which is one of reference values in [21] and shows quite good ranging accuracy in our analysis. The reference RSS was set as the RSS at the reference distance of 1 m for the ray-tracing simulation and 1.6 m for the real site, which has restricted areas near some APs in the hospital. Additionally, we compared some existing algorithms that improved range based localization. The method in [63] is the on-site channel estimation method based on sampled information from communication between APs, and the method in [66] is the weighted least square method, which considers that a weak RSS is likely to be a measure of the NLOS environment and it is less accurate to use RSS ranging. Moreover, the method in [70] induces positioning accuracy gain by optimizing the path loss exponent.

For the overlapped multi-state PLM, I consider two cases with 4 and 8 states, respectively. The PLM parameters η and β of each state can be defined based on background knowledge about indoor propagation channel and previous research [21–23]. The pathloss exponent η can be determined in the range of 2 to 3.5 and the β can be set taking into account the attenuation of obstructions. In this study, I proposed parameter sets for 4 and 8 states PLM as a reference. The parameters for the ray-tracing based simulation environment and for the real-site experiments are shown in Tables 3.2 and 3.3, respectively. I designed almost the same parameter sets to be used for both situations. Some differences in $p(d_0)$ and β betIen Table 3.2 and Table 3.3 comes from the difference in the transmit poIr of the APs and the reference distance. To apply the proposed GA-based search algorithm, the state of each model is binary encoded to the gene code as shown in Tables 3.2 and 3.3.

Table 3.2: Path loss parameters for the ray-tracing simulation

Case	State	$p(d_0)$	η	β	Gene code
Conventional PLM	LOS	-19	2	0	0
	NLOS	-9	3.5	0	1
4-state PLM	1	-19	2	0	00
	2	-14	3.2	0	01
	3		3.2	2	10
	4		3.2	6	11
8-state PLM	1	-19	2	0	000
	2		2	2	001
	3		2.2	5	010
	4	-12	3.2	0	011
	5		3.3	2	100
	6		3.3	4	101
	7		3.5	6	110
	8		3.5	8	111

Table 3.3: Path loss parameters for the experiments

Case	State	$p(d_0)$	η	β	Gene code
Conventional PLM	LOS	-39	2	0	0
	NLOS	-35	3.5	0	1
4-state PLM	1	-39	2	0	00
	2	-31	3.2	0	01
	3		3.2	7	10
	4		3.2	12	11
8-state PLM	1	-39	2	0	000
	2		2	2	001
	3		2.2	2	010
	4	-34	3.2	0	011
	5		3.3	2	100
	6		3.3	4	101
	7		3.5	2	110
	8		3.5	4	111

3.4.1 Numerical simulation

Fig. 3.5 represents the 3D modeling environment and a top view of the simulation space. I modeled an indoor space of 40 m $\times$ 32 m, whose structure was mainly composed of concrete walls, glass windows, and iron doors. For generating RSS vectors, I assume that the APs are installed at the 12 locations indicated by red diamonds in the top view of Fig. 3.5, where $N = 12$. To reflect cases in various channel condition, 3381 uniformly distributed points in the space were tested. The distance between each test point is approximately 0.6 m. We assumed a WLAN system, particularly commercial Wi-Fi network whose center frequency is 2.4 GHz [74], and set a transmit power of 20 dBm, center frequency of 2.4 GHz. In the simulation, I assumed a noise floor of -65 dBm which makes the dynamic range of the RSS similar to that of real on-site experiments.

Fig. 3.6 (a) shows distance versus RSS data. LOS with $\eta_0 = 2$ is represented as a red line and NLOS with $\eta_1 = 3.5$ is represented as a blue line based on the 802.11Tgn standard in [21], whose parameters are shown in the 2-slope PLM row in Table 3.2. Since the LOS / NLOS condition is mixed with short distances and additional losses due to multiple walls, there are limitations to approximating the PLM as simple 2-slope model. Particularly, the 2-slope model cannot account for NLOS condition. I consider 4-state and 8-state PLMs like (3.10) with the corresponding parameters given in Table 3.2. Fig. 3.6 (b) represents the superposition of 8 potential PLMs. These 8 potential PLMs also do not cover all channel conditions, but they can effectively improve the position estimation accuracy by considerably reducing the distance estimation error when proper potential PLMs are matched. Since it is difficult to distinguish the channel state from the RSS of one AP, it can be inferred that the channel state combination and distance must be estimated based on the consistency in the positioning stage.

The root mean square error (RMSE) of the position resulting from the ILS method with conventional PLM, and the exhaustive search in Algorithm 1 and GA based search in Algorithm 2 for 4-state and 8-state PLMs are compared to evaluate their

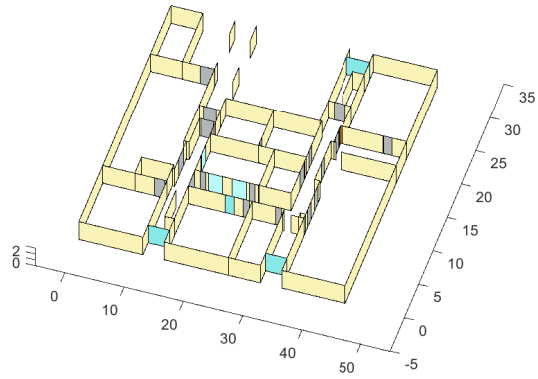

(a)

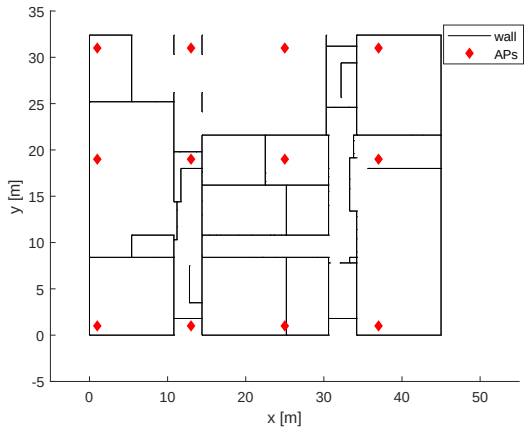

(b)

Figure 3.5: Simulation environment utilized in ray-tracing: (a) 3D view and (b) Top view.

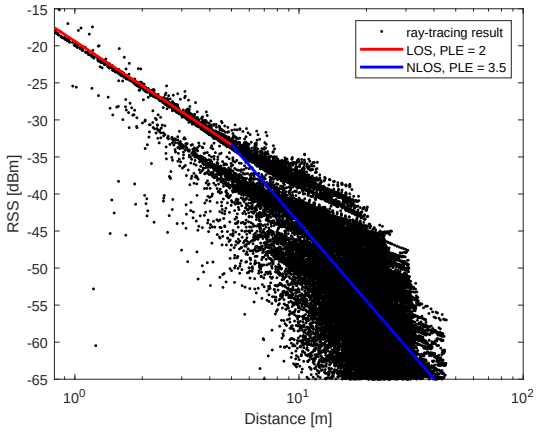

(a)

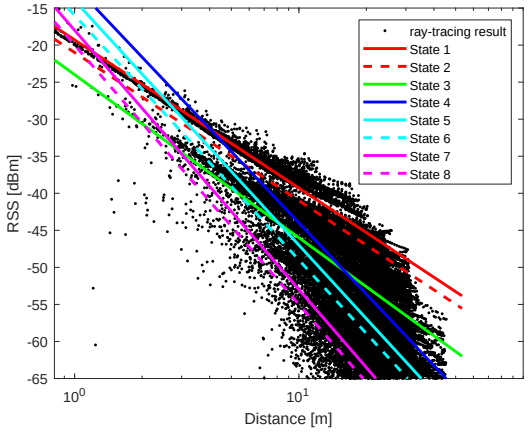

(b)

Figure 3.6: Path loss modeling for ray-tracing simulation: (a) Conventional 2 slope model, and (b) Proposed 8 states model.

performance. Fig. 3.7 shows the empirical cumulative distribution function (ECDF) of RMSE for each benchmark. The statistical results for the position error are summarized in Table 3.4. Numerically, when finding the optimal solution using the 4-state PLM, the average RMSE of the proposed method is improved by 7.7% compared to that when using the conventional PLM. In terms of accuracy, the exhaustive and GA-based search methods show similar result with the 4-state PLM as shown in Table 3.4. For the 4-state PLM, even the mean position error using the GA-based search method is slightly lower than that using exhaustive search. Due to the imperfection of the PLM, the exhaustive search method does not guarantee the best result. It can be interpreted that the results from exhaustive search and the GA based search are substantially similar within the error range. The proposed GA method with the 8-state PLM shows the best RMSE accuracy with an average of 3.38 m, which is a 23.9% improvement over the results obtained using the ILS method with conventional PLM. The result also showed good performance when the method in [63] or [66] was applied in the simulation environment. The localization algorithm with channel parameter calibration in [63] and the weighted least square method in [66] can improve RMSE accuracy up to an average of 3.66 m and 3.79 m, respectively. However, the proposed method considering the multi-state PLM showed an even better performance, with an average of 3.38 m. The method in [70] exhibits a poor localization performance. It seems that increasing the positioning accuracy by optimizing the common PLE proves to be difficult in a complex indoor environment.

To examine the statistical validation of the simulation results, I verified whether the differences in the positioning error set of each algorithm were significant using Welch's t-test [75]. These analyses showed that there were significant differences in all the results of the algorithms, except for the comparison result of the algorithm using exhaustive search and the algorithm using GA-based search. These results justify that the proposed GA-based localization algorithm can derive the same results as the exhaustive search method.

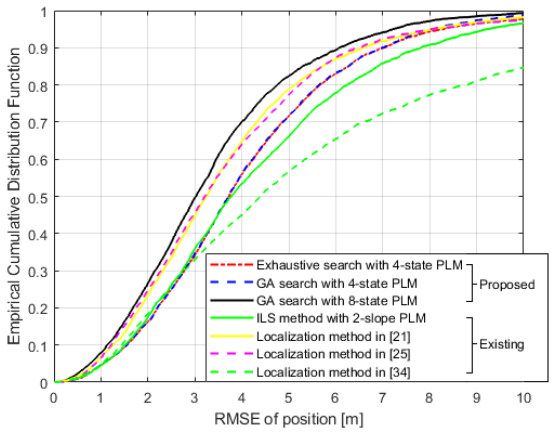

Figure 3.7: Positioning accuracy in simulation using each method.

Table 3.4: Position errors using ray-tracing based simulations

Positioning method	RMSE [m]		
	50%-tile	90%-tile	Mean
ILS method with Conventional PLM	3.78	7.81	4.44
Exhaustive search with 4-state PLM	3.73	7.02	4.10
GA search with 4-state PLM	3.69	7.08	4.08
Exhaustive search with 8-state PLM	-	-	-
GA search with 8-state PLM	3.01	6.15	3.38
Localization method in [63]	3.25	6.59	3.66
Localization method in [66]	3.21	6.49	3.79
Localization method in [70]	4.39	12.54	6.18

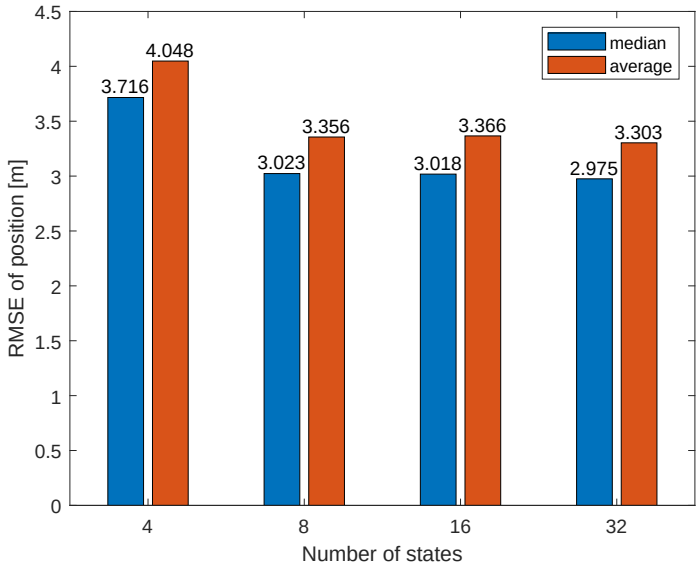

Figure 3.8: Positioning accuracy according to the number of states.

Although the increased number of states results in the improvement in positioning accuracy, there are some limitations. Fig. 3.8 depicts the result of the simulation, showing the accuracy according to the number of states of the proposed algorithm. In terms of the median and average of the positioning error, the positioning accuracy was saturated beyond the 8-state PLM. I expect that the proposed algorithm with the 8-state PLM can demonstrate an acceptable positioning performance in a typical indoor environment.

The computational complexities of the ILS and the proposed methods are presented in Table 3.1. For the 4-state PLM, the proposed exhaustive search method needs calculations up to $4^{12} = 16,777,216$ times that of the pimple ILS method, whereas the 8-state PLM requires calculations up to $8^{12} > 6 \times 10^{10}$ times that of the simple ILS method, which is not reasonable for direct calculation. I restrict the computational cost of the proposed GA method to less than 2000 times that of ILS method with the simple PLM by adjusting the termination condition. In fact, the algorithm required an

average of 500 times the computational cost compared to the conventional method. This can be regarded to make the algorithm sufficiently usable on a mobile device, and the proposed method has confirmed feasibility.

3.4.2 Experimental results

For more thorough verification, I evaluated the proposed localization algorithm with real site experiments. Fig. 3.9 shows the floor plan of the experimental site, which was an emergency room of a general hospital in Seoul, South Korea. The interior is a complex indoor environment that is divided by several walls and contains various obstacles such as beds, desks, and medical devices. Since the emergency room operates 24 h a day, experiments were conducted in a space that always had moving people. The APs for RSS collection are model-S600 manufactured by AIRTMS in South Korea. Total 7 APs were installed at locations marked with a blue star in Fig. 3.9. Measurements were performed in a hand held state at each point indicated by a red dot. In the measurement experiment, smartphones such as the Apple iPhone 6, Samsung Galaxy Note 4, and LG G6 were used. Both the APs and smartphones are commercially off-the-shelf products that support 802.11n standard WLAN communication. The distance between each test point is approximately 1.5 m. In the experiment, the mobile devices broadcast Wi-Fi packets and the installed APs capture it at the same time. I post-processed the RSS data based on the recorded mac address and time contained in the packet. The frequency of capturing packets depends on the communication link quality. Consequently, 3 to 7 APs were connected at each point, and 3 to 10 RSS samples per second were measured for each AP. In order to mitigate the effects of small scale fading, the average value of RSS measured for a few seconds was used. In a real environment, measurements are noisy compared to simulations because antenna orientation, obstruction, and shadowing by moving humans, device inequality, and other anomalies make the channel more diverse. In addition, because RSS of different mobile devices were fused, the measured data includes errors according to the characteristics of each device. Although I used

three different types of smartphone, the error is relatively small compared to shadowing and fluctuation caused by the direction of the device, the structure of the wall, and obstacles. Therefore, I did not make corrections for mobile devices in this experiment. If the RSS error caused by the characteristic of the device becomes significant in some cases, it can be expected that that will also be corrected via proper channel state selection of the proposed algorithm. By using the measured RSS vectors at each point, the results of the localization algorithms are analyzed. The PLM parameters for localization algorithm are presented in Table 3.3.

As RSSs from up to $N = 7$ APs are available, for the 4-state PLM, the exhaustive search method requires $4^7 = 16,384$ times the calculations required for the simple ILS methods; similarly, the 8-state PLM requires $8^7 = 2,097,152$ times the calculations. When GA is applied, it is possible to obtain a similar accuracy as that of the exhaustive search, while limiting the calculations amount to an average of 300 times and up to 1000 times the calculations required simple ILS method, by setting termination conditions.

The results of applying the proposed positioning method to the measured 70 points are shown in Fig. 3.10, and Table 3.5 shows some key values regarding the positioning results in real site experiments. The proposed methods considering multi-state PLM can reduce positioning error considerably. The proposed GA method shows a similar positioning accuracy as that of the exhaustive search method. By using the GA method with 8-state PLM, it was possible to obtain a mean RMSE of 1.92 m, which is 31.4% better than that obtained using the simple ILS method with 2-slope PLM. In particular, at 50% or more points, an error level of 1.67 m or less was obtained in the GA method with 8-state PLM.

In the real-site experiment, the result when the method in [63] was applied exhibited the worst positioning performance. This implies that the PLM parameter calibration failed in this environment. The method depends on the number and placement of APs and the structure of the indoor environment. As shown in Fig. 3.9, the emergency

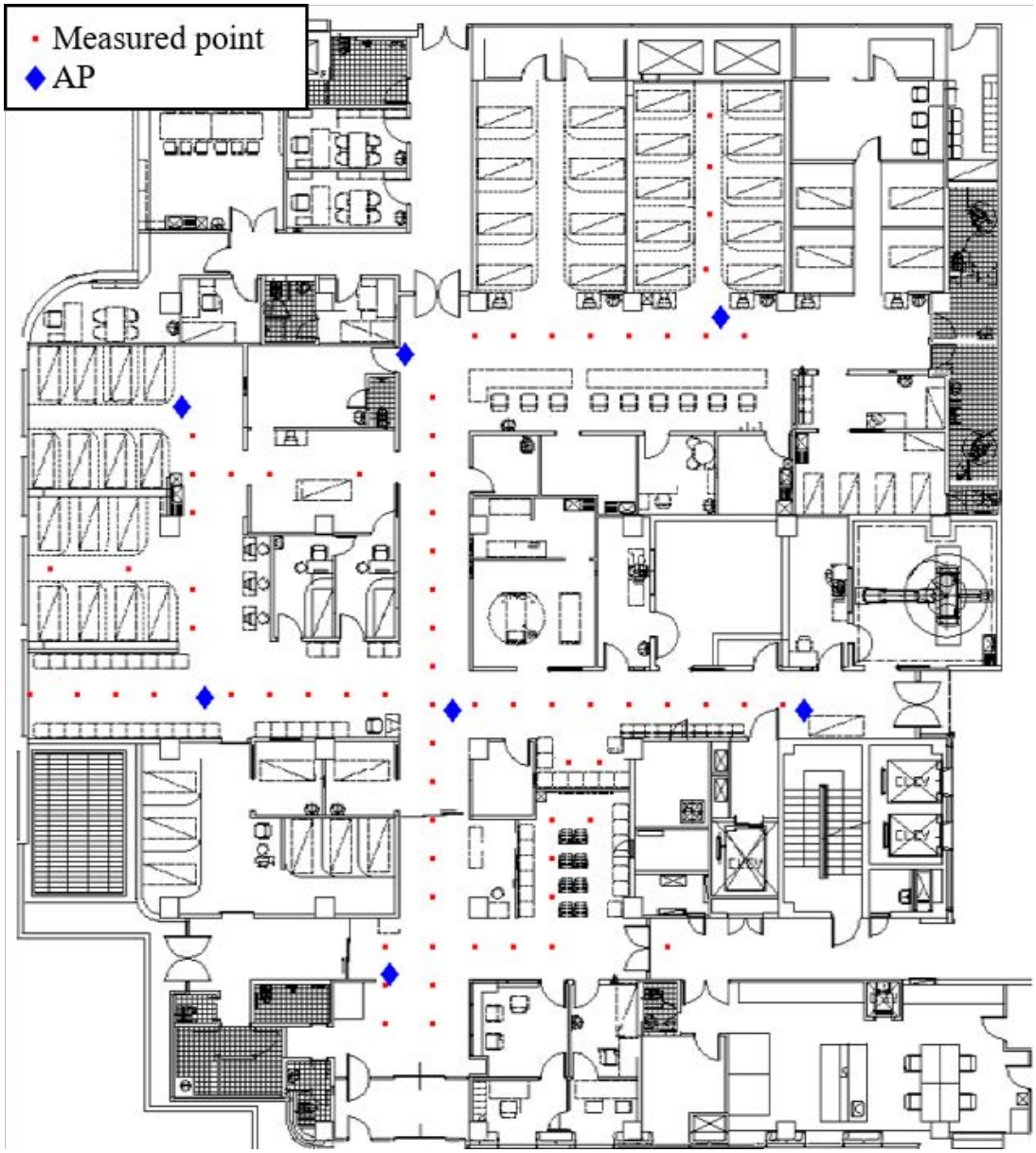

Figure 3.9: Floor plan of the experiment site.

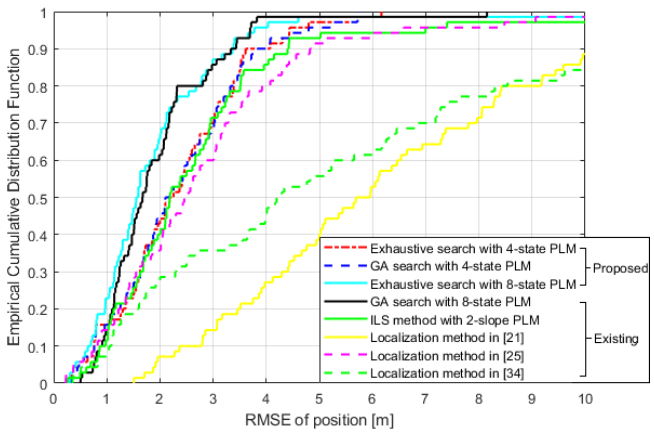

Figure 3.10: Positioning accuracy in real site experiments using each method.

room has long hallways, and most of the measuring points have more than one LOS connection and many NLOS connection with APs. It can be inferred that there are many situations where the LOS and NLOS links are mixed for a moment. The method in [63] may worsen the positioning performance as the channel parameters in LOS and NLOS are extremely different. The other methods in [66] and [70] also suffered performance degradation in the complex indoor environment. Conversely, the performance gain of the proposed method is maximized when the LOS and NLOS paths are mixed in the connection between the target node and each AP by considering the multi-stage PLM and by determining the best combination of PLMs.

Numerically, the position accuracy of the experimental result is higher than that of the simulation. This is because the simulation assumes more various NLOS conditions than in the real site and covers all regions including areas that are hard to accurately positioning such as points close to the border of the building. Practically, the expected positioning accuracy depends on APs deployment and objective area [39]. Notably, the performance improvements compared to other existing methods are quite substantial for both cases. This is meaningful because it verifies the generality of the proposed algorithm. The ray-tracing based simulation and real site experimental results both show

Table 3.5: Position errors for real site experiments

Positioning method	RMSE [m]		
	50%-tile	90%-tile	Mean
ILS method with Conventional PLM	2.19	4.41	2.80
Exhaustive search with 4-state PLM	2.22	3.53	2.34
GA search with 4-state PLM	2.29	3.48	2.41
Exhaustive search with 8-state PLM	1.57	3.37	1.90
GA search with 8-state PLM	1.67	3.38	1.92
Localization method in [63]	5.82	10.64	6.28
Localization method in [66]	2.50	4.85	2.80
Localization method in [70]	4.24	11.40	6.04

remarkable improvements in positioning accuracy considering the proposed localization method.

3.5 Summary

In this paper, I proposed a localization method with an overlapped multi-state PLM in indoor environments. The proposed algorithm estimates the location based on the combination of multiple candidates for pathloss model groups to improve the ranging and localization accuracy. Because the main limitation for improving accuracy was the increase in computational amount, the GA-based search is used to reduce the computational complexity of the optimal search method. The proposed GA method derives near-optimal solution with similar accuracy as that of the exhaustive search method and dramatically reduced computations. The effectiveness of the proposed localization method was verified through ray-tracing simulations for indoor environments. Via

experiments in an emergency room of a hospital, the proposed method showed a considerable performance improvement compared to other existing methods in localization accuracy when applied to a situation using an off-the-shelf smartphone. Because it uses a snapshot of the RSS vector at a certain instant in time, the proposed method has an advantage when used in the event of sporadic communication, where tracking-based correction techniques are difficult to apply. Furthermore, this method would be useful to determine the positions of communication nodes or indoor objects and can be applied to communication systems as long as the received signal power is measured properly.

As they have minimal need for offline stage or site surveys, it is possible to set multi-state PLM considering indoor environments. The proposed 8-state PLM parameters can serve as a guideline for a typical office or emergency room environment and would be applicable to similar indoor environments with little adjustments. It is also expected to accelerate the practical use of range-based positioning techniques using RSS by minimizing the errors caused by RSS fluctuation in existing studies. In future studies, I plan to conduct further verification of the proposed method using measurement in diverse indoor environments.

Chapter 4

Indoor User Tracking with Self-calibrating Range Bias Using FTM Protocol

4.1 Motivation

Recently, there are many research about indoor localization techniques using built-in sensors of smartphones and Wi-Fi system. In particular, a round trip time-based ranging method using fine timing measurement (FTM) can achieve meter-level accuracy. In particular, combined with pedestrian dead reckoning (PDR), it is possible to improve the positioning accuracy in the extended Kalman filter (EKF)-based tracking algorithm. However, in the indoor environment, since LOS is hard to be secured due to obstacles, the measured ranging results are prone to be positively biased. In addition, an unexpected error depending on the device types brings about outlier and degrades the tracking accuracy. These practical ranging errors are the major challenge in tracking the indoor location. In this study, I designed the EKF-based algorithm that adaptively removes outlier and corrects the ranging bias. First, the FTM ranging result of each AP is pre-filtered using the PDR-based trajectory estimation. This method removes the influence of outliers caused by hardware imperfections or incompatibility. In addition, ranging errors due to multipath effects are modeled, and correction

parameters are estimated for each AP. The EKF was designed to reflect the ranging error characteristics that change according to the location change of the user. To verify the performance of the proposed tracking algorithm, I conducted experiment in the academic building at Seoul national university. The experiments were conducted with non-homogeneous AP set, and the performance of the proposed algorithm was evaluated. The remainder of this paper is organized as follows: In the next section, we present FTM protocol-based ranging and our system model. In Section III, we propose a localization algorithm based on EKF designed to remove outlier and adaptively compensate FTM result. Section IV shows a performance analysis of the proposed algorithm using indoor experiments.

4.2 Preliminary

4.2.1 FTM ranging

The FTM protocol in IEEE 802.11-2016 standard provides a distance estimation result based on round trip time through message frame exchange of devices supporting the protocol. The overall messave flow is shown in fig. 4.1. In a typical scenario, a user device is an initiating station (ISTA) and a Wi-Fi access point (AP) serves as a responding station (RSTA). The ISTA and the RSTA each use their own local clocks to record the packet transmission/reception time, and after a series of processes, the estimated distance $\hat{d}$ between the two devices is expressed as follows.

$$\hat{d} = \frac{c}{2}\left\{(t_4 - t_1) - (t_3 - t_2)\right\}, \tag{4.1}$$

where c represent the speed of the light. If the burst mode of the FTM protocol is used, more accurate results can be obtained by repeating the process B times. An error may occur in the ranging result measured in this way due to the absence of the LOS path or failure of direct path detection by the multipath propagation. Therefore, the ranging result typically has a positive bias. However, as a practical issue, the user

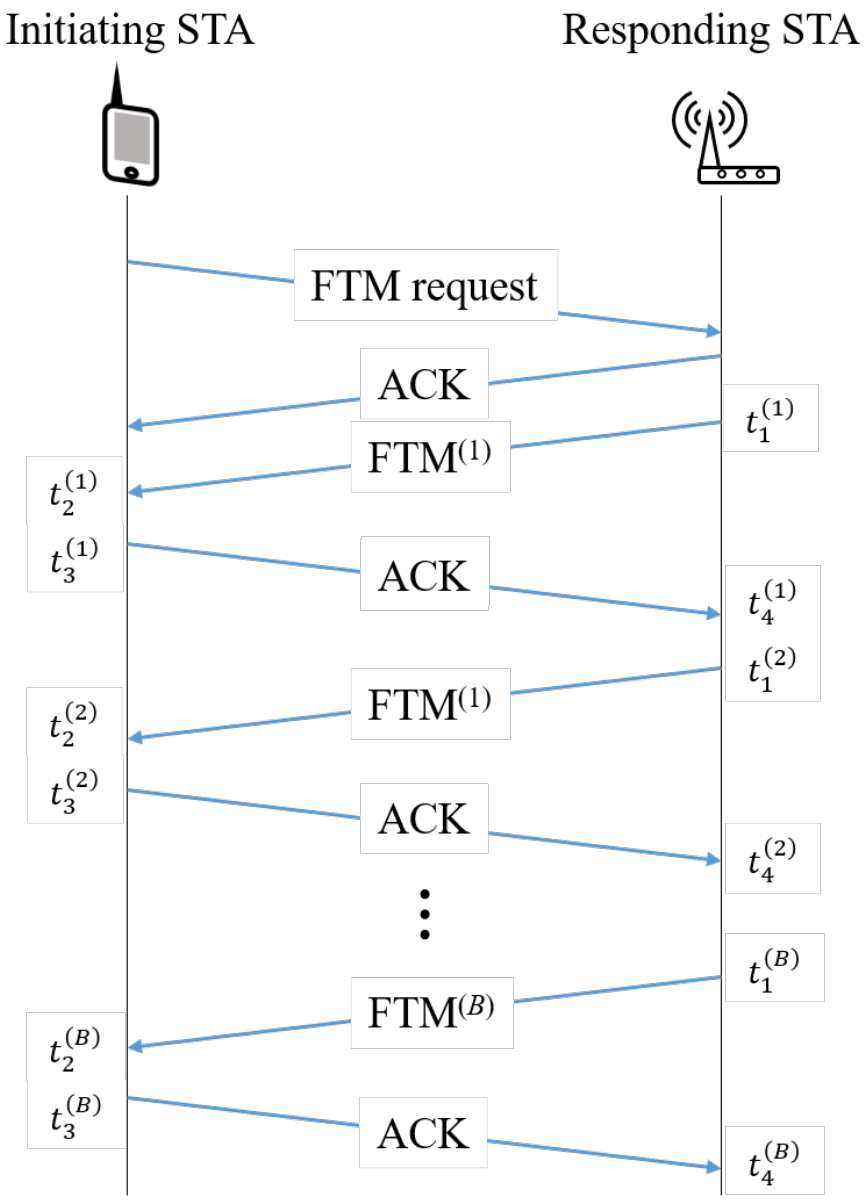

Figure 4.1: Fine timing measurement protocol.

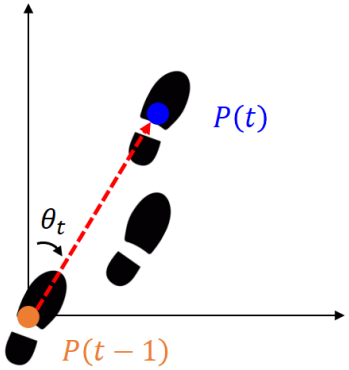

Figure 4.2: Pedestrian dead reckoning concept.

device may receive a distance value even shorter than the actual distance due to the device compatibility or internal software problems. In this study, to compensate for the bias error, I model the FTM ranging result $\hat{d}_n$ measured for the actual distance d_n between the n-th AP and the user device as follows:

$$\hat{d}_n = \alpha_n \cdot d_n + \beta_n \tag{4.2}$$

4.2.2 PDR-based trajectory estimation

By using the built-in IMU of the smartphone, it is possible to detect the step of a user and estimate the trajectory by combining it with the direction information of the device. Fig. 4.2 is a basic conceptual diagram of PDR based trajectory estimation. The change in the position of the pedestrian can be expressed as follows.

$$P(t) = P(t-1) + L \cdot \begin{bmatrix} \sin(\theta_t) \\ \cos(\theta_t) \end{bmatrix}, \tag{4.3}$$

where $P(t)$, θ_t, and L represent the position, heading, the step length of the user at time t, respectively. The trajectory estimated using PDR shows high accuracy for a

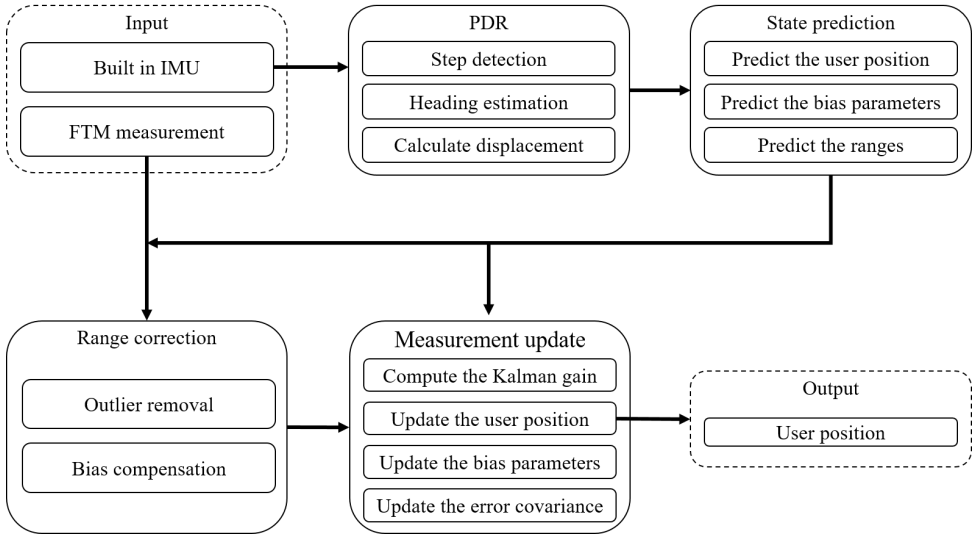

Figure 4.3: Overall flow of the proposed method.

short time, but errors occur due to incomplete estimation of step length and heading, and this accumulates and the difference from the actual path increases as time goes by. Therefore, the PDR is not suitable to be used stand-alone, and it is possible to increase the tracking accuracy by combining it with the FTM result. I use only the displacement $\Delta P(t) = P(t) - P(t-1)$ in this study.

4.3 EKF design for adaptive compensation of ranging bias

To track the trajectory of the user in the indoor, an EKF-based tracking algorithm is designed. The overall flow of the proposed method is depicted in fig. 4.3. I denote $[x, y]^{\mathrm{T}}$ and $[x_n, y_n]^{\mathrm{T}}$ as the coordinates of the device and n-th AP among total N APs, respectively. Then, a state vector $\mathbf{z}$ is defined as follows

$$\mathbf{z} = [x, y, \alpha_1, \ldots, , \alpha_n, \beta_1, \ldots, \beta_n]^{\mathrm{T}} \tag{4.4}$$

For the initial state, the covariance matrix is given as

$$\mathrm{P} = diag(\sigma_x^2, \sigma_y^2, \sigma_{\alpha_1}^2, \ldots, \sigma_{\alpha_n}^2, \sigma_{\beta_1}^2, \ldots, \sigma_{\beta_n}^2) \tag{4.5}$$

State transition model is expressed by

$$\begin{aligned}\hat{\mathbf{z}}^{(k|k-1)} &= f(\hat{\mathbf{z}}^{(k-1|k-1)}, P(k), \mathbf{w}^{(k)}) \\ &= [(x^{(k-1)} + \Delta x^{(k)}), (y^{(k-1)} + \Delta y^{(k)}), \alpha_1^{(k-1)}, \cdots, \alpha_n^{(k-1)}, \beta_1^{(k-1)}, \cdots, \beta_n^{(k-1)}]^{\mathrm{T}} \\ &+ \mathbf{w}^{(k)},\end{aligned} \tag{4.6}$$

where $[\Delta x^(k), \Delta y^(k)]^{\mathrm{T}}$ is the displacement of the user estimated from PDR, and $\mathbf{w}$ represents the state transition error which is a zero mean multivariate Gaussian vector. The covariance matrix is updated as follow:

$$\mathrm{P}^{(k|k-1)} = \mathrm{F}^{(k)}\mathrm{P}^{(k-1|k-1)}(\mathrm{F}^{(k)})^{\mathrm{T}} + \mathrm{Q}^{(k)}, \tag{4.7}$$

where $\mathrm{Q}^{(k)} = E[\mathbf{w}^{(k)}(\mathbf{w}^{(k)})^{\mathrm{T}}]$ and

$$\mathrm{F}^{(k)} = \frac{\partial f}{\partial z}|_{\mathbf{z}=\hat{\mathbf{z}}^{(k-1|k-1)}} = \mathrm{I}_{(2+2N)} \tag{4.8}$$

FTM result vector is represented as follow:

$$\mathrm{d}^{(k)} = h(\mathrm{z}) + \mathbf{v}^{(k)} = \begin{bmatrix} \alpha_1^{(k)} \cdot \sqrt{(x^{(k)} - x_1)^2 + (y^{(k)} - y_1)^2} + \beta_1^{(k)} \\ \vdots \\ \alpha_n^{(k)} \cdot \sqrt{(x^{(k)} - x_n)^2 + (y^{(k)} - y_n)^2} + \beta_n^{(k)} \end{bmatrix} + \mathbf{v}^{(k)}, \tag{4.9}$$

where $\mathbf{v}^{(k)}$ represents the measurement error which is assumed a zero mean multivariate Gaussian vector, whose covariance matrix $\mathrm{R}^{(k)} = E[\mathbf{v}^{(k)}(\mathbf{v}^{(k)})^{\mathrm{T}}]$.

Then, the innovation is expressed as follow:

$$\zeta^{(k)} = \mathrm{d}^{(k)} - h(\hat{\mathrm{z}}^{(k|k-1)}) \tag{4.10}$$

In this step, we applied measurement pre-filtering by discarding FTM result of AP where the difference between the predicted and measured distances was greater than the threshold value. In this way, the outliers that occur in FTM results can be removed. The Kalman gain, updated state, and the updated covariance matrix can be calculated as follows:

$$\mathrm{K}^{(k)} = \mathrm{P}^{(k|k-1)}(\mathrm{H}^{(k)})^{\mathrm{T}}(\mathrm{H}^{(k)}\mathrm{P}^{(k|k-1)}(\mathrm{H}^{(k)})^{\mathrm{T}} + \mathrm{R}^{(k)})^{-1} \tag{4.11}$$

$$\mathrm{z}^{(k|k)} = \mathrm{z}^{(k|k-1)} + \mathrm{K}^{(k)}\zeta^{(k)} \tag{4.12}$$

$$\mathrm{P}^{(k|k)} = (\mathrm{I} - \mathrm{K}^{(k)}\mathrm{H}^{(k)})\mathrm{P}^{(k|k-1)} \tag{4.13}$$

4.4 Performance evaluation

4.4.1 Experimental scenario

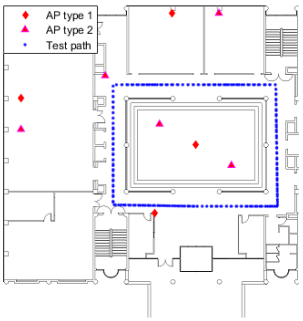

(a)

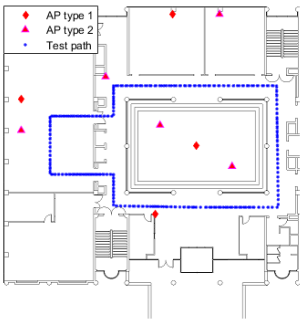

(b)

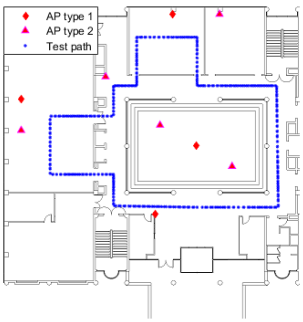

(c)

Figure 4.4: Experiment environment and path for (a) scenario 1 and (b) scenario 2 (c) scenario 3.

To verify the performance of the proposed tracking algorithm, I conducted experiment in the academic building at Seoul national university. The floor plan and ground truth paths of 3 scenarios are shown in fig. 4.4. The size of the area was 34 meters wide and 36 meters long. The scenario 1 is a corridor only, and the scenarios 2 and 3 are paths through a room. In addition to walls, there was an environment in which LOS/NLOS conditions are mixed due to pillars or obstacles in the building. Two types of Wi-Fi APs (type1 - Asus RT-ACRH13, type2 - Google WiFi) were placed in total 9 locations, and the user equipped with a commercial smartphone (Pixel 4a of the Google). The user started from the lower center of the test path and walked 2 laps counterclockwise at a constant speed. The IMU operates at about 100Hz, and one set of FTM results using the 80MHz bandwidth was recorded about every second.

4.4.2 Experimental results

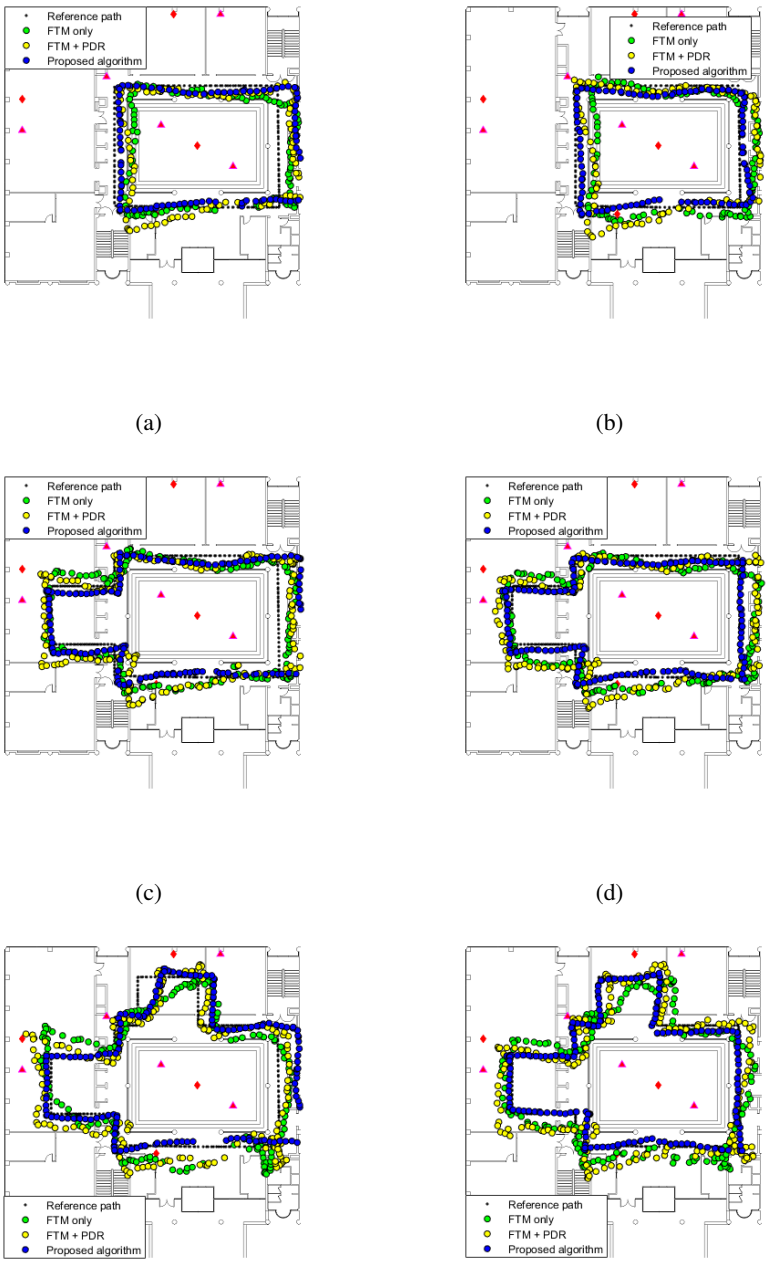

Figure 4.5: Estimated user path for (a) scenario 1 - first lap (b) scenario 1 - second lap (c) scenario 2 - first lap (d) scenario 2 - second lap (e) scenario 3 - first lap and (f) scenario 3 - second lap.

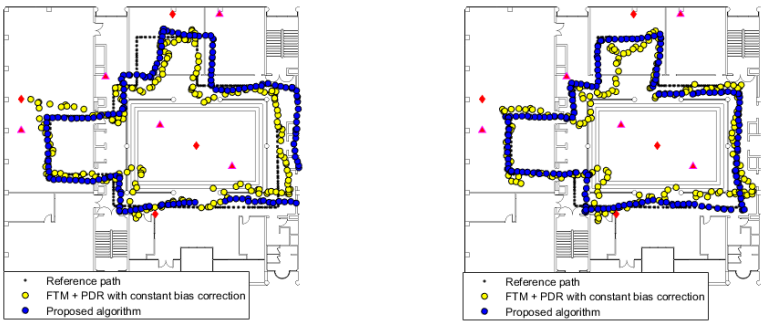

(a) (b)

Figure 4.6: Estimated user path for (a) scenario 3 - first lap and (b) scenario 3 - second lap.

Fig. 4.5 shows the estimated path results for the test scenarios. The initial values alpha and beta of the ranging bias parameter were set to 1 and 0, respectively. In each scenario, the starting location was incorrectly estimated due to an initial ranging error, and the route of some sections was not accurately estimated on the first lap. However, on the second lap, it is shown that the trajectory of the user was tracked accurately in most areas when the proposed algorithm is applied.

Fig. 4.6 shows the estimated path results for the test scenarios 3. As a comparison of the proposed method, the yellow trajectory shows the result when the constant bias correction is applied. The bias value was determined as the average of the measured distance error. Although the constant bias correction method improves positioning accuracy, it has limitations because it does not reflect the ranging error that vary by each AP and NLOS condition.

Table 4.1 shows the average of RMSE between the ground truth location and the estimated location coordinates for each scenario. When the proposed algorithm is applied, the bias characteristic is estimated as the path becomes longer, thereby it reduces the ranging error and improves the tracking accuracy. It is verified that the sub-meter level accuracy is achieved in the second round of all scenario paths.

Fig. 4.7 shows the histograms of the error between the true distance and the estimated distance between the APs and the user device during the second lap of each scenario. The red line is the Gaussian distribution fit to the data. When only outlier removal was performed, the average value of the ranging error was 1.28 m, 1.41 m, and 1.20 m for each scenario. The average of the ranging error corrected with the parameters estimated through the proposed method was 0.86 m, 0.66 m, and 0.45 m, which was reduced by 44%, 54%, and 65% compared to the previous one. Additionally, as shown in Fig. 4.7, the error distribution is closer to a Gaussian distribution than before.

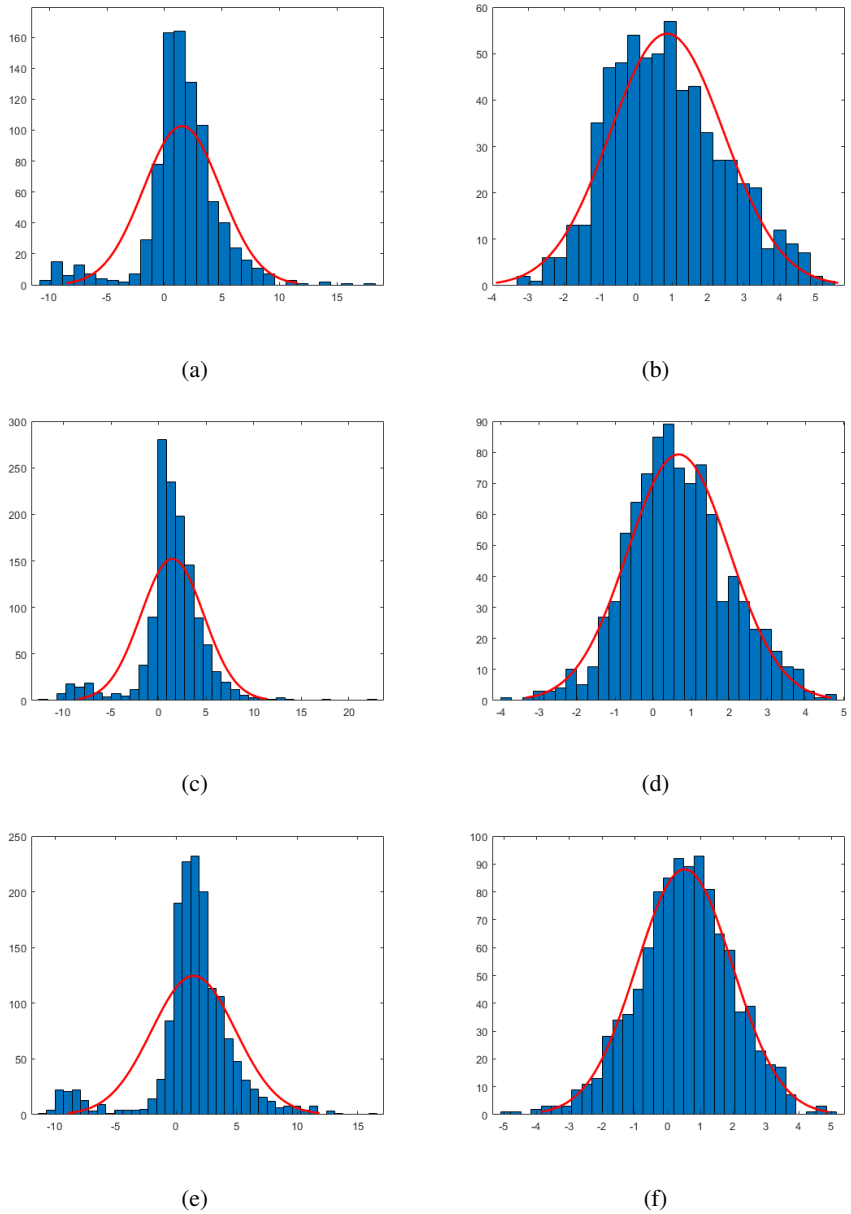

Figure 4.7: Ranging error histogram of the second lap with a Gaussian distribution fit (a) scenario 1 - before correction (b) scenario 1 - after correction (c) scenario 2 - before correction (d) scenario 2 - after correction (e) scenario 3 - before correction and (f) scenario 3 - after correction.

Table 4.1: Average RMSE of the user positions

RMSE [m]		FTM only	FTM+PDR	FTM+PDR with constant bias	Proposed method
scenario 1	1-st lap	2.38	1.78	1.25	1.35
	2-nd lap	2.14	1.77	1.24	0.596
scenario 2	1-st lap	1.81	1.53	1.13	1.17
	2-nd lap	1.94	1.71	1.14	0.650
scenario 3	1-st lap	2.36	1.66	1.21	1.31
	2-nd lap	2.00	1.51	1.15	0.575

4.5 Summary

In this study, we proposed an EKF-based algorithm with adaptive compensation of ranging bias to track the indoor location of the smartphone user. We remove outlier from the FTM result for each AP by comparing it with the predicted value from previous status and the PDR-based displacement. Additionally, the bias of the FTM result with each AP was modeled as a changing with time. In the end, the user positioning accuracy is improved by correcting the FTM ranging result. Experiments using commercial smartphone and Wi-Fi 6 routers verified that the bias of the FTM result of each AP was reduced by 65.60% compared to the raw measurement during a lap in the scenario path, and the ranging error distribution showed to be closer to the zero-mean Gaussian distribution. The final positioning RMSE was obtained at 0.58 m, which is 54.18% smaller than when without the range compensation. The proposed algorithm makes it possible to track the user's location with sub-meter accuracy. In the future, if the bias characteristic for each AP estimated by the user is provided to the next user, then it may be possible to further improve the localization accuracy.

Chapter 5

Conclusion

In this dissertation, I investigated Wi-Fi based indoor localization methods. All of the proposed methods are designed to consider a practical indoor environment and the indoor channel characteristic. Due to the many obstacles and complex structure in the indoor, ranging with radio propagation is suffered from multipath whether using RSS or FTM result. At the beginning of the study, I proposed a hybrid localization algorithm that replaces only the ranging part of the existing range-based localization method with a deep regression model that uses data-driven learning. For the ranging part, the accuracy of distance estimation in an indoor NLOS environment is improved by using the dual-band RSS, and this is designed to cover various cases by using regression with a neural network. The improvements in the ranging and positioning accuracy of the proposed method were verified through a ray-tracing-based simulation for general indoor spaces. Furthermore, the proposed localization method is compatible with various situations, even when the indoor structure is changed. Based on the results of ray-tracing based simulation, the use of dual-band RSS could reduce the median of positioning error up to 2.56 m, which was a 9.9% smaller error than the error obtained with the single-band RSS alone in the rule-based localization. By applying the deep regression method to the ranging part, the median error of 1.99 m was obtained, which was a 22.3% improved result compared to the rule-based method. Considering that the use

of deep regression with single-band RSS only caused 10% or less performance gain, the combination of the dual-band RSS and the deep regression method was effective in improving the accuracy of range-based localization using RSS. The robustness of the proposed method encourages the use of RSS localization because it can reduce the intensity of the site survey process. The proposed method is still promising in that a properly trained ranging model can be used even in an untrained environment. In practice, I expect to increase the learning efficiency by using a transfer learning technique that tunes the model trained through simulation with relatively small dataset from real experiments. Furthermore, extending the research to the triple-band-based ranging method is possible by utilizing 6 GHz band communication, which is expected to be supported in the Wi-Fi 6E standard. Next, I proposed a localization method with an overlapped multi-state PLM in indoor environments. The proposed algorithm estimates the location based on the combination of multiple candidates for pathloss model groups to improve the ranging and localization accuracy. Because the main limitation for improving accuracy was the increase in computational amount, the GA-based search is used to reduce the computational complexity of the optimal search method. The proposed GA method derives near-optimal solution with similar accuracy as that of the exhaustive search method and dramatically reduced computations. The effectiveness of the proposed localization method was verified through ray-tracing simulations for indoor environments. Via experiments in an emergency room of a hospital, the proposed method showed a considerable performance improvement compared to other existing methods in localization accuracy when applied to a situation using an off-the-shelf smartphone. Because it uses a snapshot of the RSS vector at a certain instant in time, the proposed method has an advantage when used in the event of sporadic communication, where tracking-based correction techniques are difficult to apply.The proposed 8-state PLM parameters can serve as a guideline for a typical office or emergency room environment and would be applicable to similar indoor environments with little adjustments. Finally, I proposed an EKF-based algorithm with adaptive compen-

sation of ranging bias to track the indoor location of the smartphone user. I remove outlier from the FTM result for each AP by comparing it with the predicted value from previous status and the PDR-based displacement. Additionally, the bias of the FTM result with each AP was modeled as a changing with time. In the end, the user positioning accuracy is improved by correcting the ranging result. Experiments using commercial smartphone and Wi-Fi 6 routers verified that the bias of the FTM result of each AP was reduced by 65.60% compared to the raw measurement during one round of the scenario path, and the ranging error distribution showed to be closer to the zero-mean Gaussian distribution. The final positioning RMSE was obtained at 0.57 m, which is 54.18% smaller than when without the range compensation. The proposed algorithm makes it possible to track the user's location with sub-meter accuracy. I expect that the proposed method in this dissertation will accelerate the practical use of range-based positioning techniques for indoor application by minimizing the errors caused by the indoor propagation.

Bibliography

[1] A. Čolaković and M. Hadžialić, "Internet of things (iot): A review of enabling technologies, challenges, and open research issues," *Computer Networks*, vol. 144, pp. 17–39, 2018.

[2] K. Cengiz, "Comprehensive analysis on least squares lateration for indoor positioning systems," *IEEE Internet of Things Journal*, pp. 1–1, 2020.

[3] X. Guo, L. Li, F. Xu, and N. Ansari, "Expectation maximization indoor localization utilizing supporting set for internet of things," *IEEE Internet of Things Journal*, vol. 6, no. 2, pp. 2573–2582, April 2019.

[4] L. Chettri and R. Bera, "A comprehensive survey on internet of things (iot) towards 5g wireless systems," *IEEE Internet of Things Journal*, 2019.

[5] Y. Li and K. Yan, "Indoor localization based on radio and sensor measurements," *IEEE Sensors Journal*, 2021.

[6] S. He and S.-H. G. Chan, "Wi-fi fingerprint-based indoor positioning: Recent advances and comparisons," *IEEE Communications Surveys & Tutorials*, vol. 18, no. 1, pp. 466–490, 2015.

[7] C. E. Galván-Tejada, J. P. García-Vázquez, J. I. Galván-Tejada, J. R. Delgado-Contreras, and R. F. Brena, "Infrastructure-less indoor localization using the microphone, magnetometer and light sensor of a smartphone," *Sensors*, vol. 15, no. 8, pp. 20 355–20 372, 2015.

[8] I. Ashraf, S. Hur, S. Park, and Y. Park, "Deeplocate: Smartphone based indoor localization with a deep neural network ensemble classifier," *Sensors*, vol. 20, no. 1, p. 133, 2020.

[9] X. Hou and J. Bergmann, "A pedestrian dead reckoning method for head-mounted sensors," *Sensors*, vol. 20, no. 21, p. 6349, 2020.

[10] A. Xiao, R. Chen, D. Li, Y. Chen, and D. Wu, "An indoor positioning system based on static objects in large indoor scenes by using smartphone cameras," *Sensors*, vol. 18, no. 7, p. 2229, 2018.

[11] M. Delamare, F. Duval, and R. Boutteau, "A new dataset of people flow in an industrial site with uwb and motion capture systems," *Sensors*, vol. 20, no. 16, p. 4511, 2020.

[12] C. Xiao, D. Yang, Z. Chen, and G. Tan, "3-d ble indoor localization based on denoising autoencoder," *IEEE Access*, vol. 5, pp. 12 751–12 760, 2017.

[13] B. Al-Madani, F. Orujov, R. Maskeliūnas, R. Damaševičius, and A. Venčkauskas, "Fuzzy logic type-2 based wireless indoor localization system for navigation of visually impaired people in buildings," *Sensors*, vol. 19, no. 9, p. 2114, 2019.

[14] F. Seco and A. R. Jiménez, "Smartphone-based cooperative indoor localization with rfid technology," *Sensors*, vol. 18, no. 1, p. 266, 2018.

[15] E. Au, "The latest progress on ieee 802.11 mc and ieee 802.11 ai [standards]," *IEEE Vehicular Technology Magazine*, vol. 11, no. 3, pp. 19–21, 2016.

[16] Y. Yu, R. Chen, Z. Liu, G. Guo, F. Ye, and L. Chen, "Wi-fi fine time measurement: Data analysis and processing for indoor localisation," *The Journal of Navigation*, vol. 73, no. 5, pp. 1106–1128, 2020.

[17] M. Ibrahim, H. Liu, M. Jawahar, V. Nguyen, M. Gruteser, R. Howard, B. Yu, and F. Bai, "Verification: Accuracy evaluation of wifi fine time measurements

on an open platform," in *In Proceedings of the 24th Annual International Conference on Mobile Computing and Networking, New Delhi, India*, 29 October-2 November 2018; pp.417-427.

[18] K. Han, S. M. Yu, S.-L. Kim, and S.-W. Ko, "Exploiting user mobility for wifi rtt positioning: A geometric approach," *IEEE Internet of Things Journal*, 2021.

[19] X. Liu, B. Zhou, P. Huang, W. Xue, Q. Li, J. Zhu, and L. Qiu, "Kalman filter-based data fusion of wi-fi rtt and pdr for indoor localization," *IEEE Sensors Journal*, vol. 21, no. 6, pp. 8479–8490, 2021.

[20] Y. Yu, R. Chen, L. Chen, G. Guo, F. Ye, and Z. Liu, "A robust dead reckoning algorithm based on wi-fi ftm and multiple sensors," *Remote Sensing*, vol. 11, no. 5, p. 504, 2019.

[21] V. Erceg, L. Schumacher, P. Kyritsi, A. Molisch, D. Baum, A. Gorokhov, C. Oestges, Q. Li, K. Yu, N. Tal *et al.*, "Ieee 802.11 tgn channel models," *document IEEE*, vol. 802, 2004.

[22] ITU-R, "Propagation data and prediction methods for the planning of indoor radiocommunication systems and radio local area networks in the frequency range 300 mhz to 450 ghz," *Recommendation ITU-R P. 1238-10*, 2019.

[23] G. T. 38.901, "Study on channel model for frequencies from 0.5 to 100 ghz," 2017.

[24] L. T. Common, "Propagation losses through common building materials 2.4 ghz vs 5 ghz," *E10589, Magis Network, Inc*, 2002.

[25] H. Obeidat, R. Asif, N. Ali, Y. Dama, O. Obeidat, S. Jones, W. Shuaieb, M. A. Al-Sadoon, K. Hameed, A. Alabdullah *et al.*, "An indoor path loss prediction model using wall correction factors for wireless local area network and 5g indoor networks," *Radio Science*, vol. 53, no. 4, pp. 544–564, 2018.

[26] X. Wang, L. Gao, and S. Mao, "Csi phase fingerprinting for indoor localization with a deep learning approach," *IEEE Internet of Things Journal*, vol. 3, no. 6, pp. 1113–1123, 2016.

[27] C. Chen, Y. Chen, Y. Han, H.-Q. Lai, F. Zhang, and K. R. Liu, "Achieving centimeter-accuracy indoor localization on wifi platforms: A multi-antenna approach," *IEEE Internet of Things Journal*, vol. 4, no. 1, pp. 122–134, 2016.

[28] W. Wang, D. Marelli, and M. Fu, "Dynamic indoor localization using maximum likelihood particle filtering," *Sensors*, vol. 21, no. 4, p. 1090, 2021.

[29] C.-M. Own, J. Hou, and W. Tao, "Signal fuse learning method with dual bands wifi signal measurements in indoor positioning," *IEEE Access*, vol. 7, pp. 131 805–131 817, 2019.

[30] Y. Agata, J. Hong, and T. Ohtsuki, "Room-level proximity detection based on rss of dual-band wi-fi signals," in *In Proceedings of the 2016 IEEE International Conference on Communications (ICC), Kuala Lumpur, Malaysia*, 23-27 May 2016; pp.1-6.

[31] H. J. Jo and S. Kim, "Indoor smartphone localization based on los and nlos identification," *Sensors*, vol. 18, no. 11, p. 3987, 2018.

[32] J. Yang, "Indoor localization system using dual-frequency bands and interpolation algorithm," *IEEE Internet of Things Journal*, 2020.

[33] L. Zhao, H. Wang, J. Wang, H. Gao, and J. Liu, "Robust wi-fi indoor localization with kpca feature extraction of dual band signals," in *In Proceedings of the 2017 IEEE International Conference on Robotics and Biomimetics (ROBIO), Macao, China*, 5-8 December 2017; pp.908-913.

[34] C. Kumar and K. Rajawat, "Dictionary-based statistical fingerprinting for indoor localization," *IEEE Transactions on Vehicular Technology*, vol. 68, no. 9, pp. 8827–8841, 2019.

[35] Y. Li, X. Hu, Y. Zhuang, Z. Gao, P. Zhang, and N. El-Sheimy, "Deep reinforcement learning (drl): Another perspective for unsupervised wireless localization," *IEEE Internet of Things Journal*, vol. 7, no. 7, pp. 6279–6287, 2019.

[36] M. Ibrahim, M. Torki, and M. ElNainay, "Cnn based indoor localization using rss time-series," in *In Proceedings of the 2018 IEEE Symposium on Computers and Communications (ISCC), Natal, Brazil*, 25-28 June 2018; pp.01044-01049.

[37] J. Liu, N. Liu, Z. Pan, and X. You, "Autloc: deep autoencoder for indoor localization with rss fingerprinting," in *In Proceedings of the 2018 10th International Conference on Wireless Communications and Signal Processing (WCSP), Hangzhou, China*, 18-20 October 2018; pp.1-6.

[38] A. Zanella, "Best practice in rss measurements and ranging," *IEEE Communications Surveys & Tutorials*, vol. 18, no. 4, pp. 2662–2686, 2016.

[39] N. Patwari, J. N. Ash, S. Kyperountas, A. O. Hero, R. L. Moses, and N. S. Correal, "Locating the nodes: cooperative localization in wireless sensor networks," *IEEE Signal processing magazine*, vol. 22, no. 4, pp. 54–69, 2005.

[40] P. Barsocchi, S. Lenzi, S. Chessa, and G. Giunta, "A novel approach to indoor rssi localization by automatic calibration of the wireless propagation model," in *In Proceedings of the VTC Spring 2009 - IEEE 69th Vehicular Technology Conference, Barcelona, Spain*, 26-29 April 2009; pp.1-5.

[41] Y. Solahuddin and R. Mardeni, "Indoor empirical path loss prediction model for 2.4 ghz 802.11 n network," in *In Proceedings of the 2011 IEEE International Conference on Control System, Computing and Engineering, Penang, Malaysia*, 25-27 November 2011; pp.12-17.

[42] H. Nurminen, J. Talvitie, S. Ali-Löytty, P. Müller, E.-S. Lohan, R. Piché, and M. Renfors, "Statistical path loss parameter estimation and positioning using rss measurements in indoor wireless networks," in *In Proceedings of the 2012 International Conference on Indoor Positioning and Indoor Navigation (IPIN), Penang, Malaysia*, 3-15 November 2012; pp.1-9.

[43] A. Bel, J. L. Vicario, and G. Seco-Granados, "Localization algorithm with on-line path loss estimation and node selection," *Sensors*, vol. 11, no. 7, pp. 6905–6925, 2011.

[44] H. T. Friis, "A note on a simple transmission formula," *Proceedings of the IRE*, vol. 34, no. 5, pp. 254–256, 1946.

[45] A. Coluccia and F. Ricciato, "Rss-based localization via bayesian ranging and iterative least squares positioning," *IEEE Communications letters*, vol. 18, no. 5, pp. 873–876, 2014.

[46] Y. He and A. Bilgic, "Iterative least squares method for global positioning system," *Advances in Radio Science: ARS*, vol. 9, p. 203, 2011.

[47] S. Ioffe and C. Szegedy, "Batch normalization: Accelerating deep network training by reducing internal covariate shift," *arXiv preprint arXiv:1502.03167*, 2015.

[48] I. Goodfellow, Y. Bengio, and A. Courville, *Deep Learning*. MIT Press, 2016, http://www.deeplearningbook.org.

[49] J.-H. Jung, J. Lee, J.-H. Lee, Y.-H. Kim, and S.-C. Kim, "Ray-tracing-aided modeling of user-shadowing effects in indoor wireless channels," *IEEE transactions on antennas and propagation*, vol. 62, no. 6, pp. 3412–3416, 2014.

[50] J.-Y. Lee, Y. Kim, S. Lee, W. Cho, and S.-C. Kim, "Estimation of room shape using radio propagation channel analysis," *IEEE Sensors Journal*, vol. 19, no. 24, pp. 12 316–12 324, 2019.

[51] P. Bahl and V. N. Padmanabhan, "Radar: An in-building rf-based user location and tracking system," in *Proceedings IEEE INFOCOM 2000. Conference on Computer Communications. Nineteenth Annual Joint Conference of the IEEE Computer and Communications Societies (Cat. No. 00CH37064)*, vol. 2. Ieee, 2000, pp. 775–784.

[52] M. Youssef and A. Agrawala, "The horus wlan location determination system," in *Proceedings of the 3rd international conference on Mobile systems, applications, and services*, 2005, pp. 205–218.

[53] S. B. Keser, U. Yayan, A. Yazici, and S. Gunal, "A priori verification and validation study of rfkon database," *International Journal of Computer Science: Theory and Application*, vol. 5, pp. 20–27, 2016.

[54] J. Choi, Y.-S. Choi, and S. Talwar, "Unsupervised learning techniques for trilateration: From theory to android app implementation," *IEEE Access*, vol. 7, pp. 134 525–134 538, 2019.

[55] N. Dvorecki, O. Bar-Shalom, L. Banin, and Y. Amizur, "A machine learning approach for wi-fi rtt ranging," in *Proc. Int. Tech. Meeting Inst. Navigat.*, 2019, pp. 435–444.

[56] H. Xia, J. Zuo, S. Liu, and Y. Qiao, "Indoor localization on smartphones using built-in sensors and map constraints," *IEEE Transactions on Instrumentation and Measurement*, vol. 68, no. 4, pp. 1189–1198, 2018.

[57] Y. Wang, X. Jia, H. K. Lee, and G. Li, "An indoors wireless positioning system based on wireless local area network infrastructure," in *6th Int. Symp. on Satellite Navigation Technology Including Mobile Positioning & Location Services*, vol. 54, 2003.

[58] B. Wang, X. Gan, X. Liu, B. Yu, R. Jia, L. Huang, and H. Jia, "A novel weighted knn algorithm based on rss similarity and position distance for wi-fi fingerprint positioning," *IEEE Access*, vol. 8, pp. 30 591–30 602, 2020.

[59] L. Zhang, Z. Chen, W. Cui, B. Li, C. Chen, Z. Cao, and K. Gao, "Wifi-based indoor robot positioning using deep fuzzy forests," *IEEE Internet of Things Journal*, 2020.

[60] F. Potorti, J. Torres-Sospedra, D. Quezada-Gaibor, A. R. Jiménez, F. Seco, A. Pérez-Navarro, M. Ortiz, N. Zhu, V. Renaudin, R. Ichikari *et al.*, "Off-line evaluation of indoor positioning systems in different scenarios: The experiences from ipin 2020 competition," *IEEE Sensors Journal*, 2021.

[61] M. Xiang, Y. Hu, and L. Li, "A connectivity based localization algorithm for sensor network," in *2011 International Conference on Network Computing and Information Security*, vol. 2. IEEE, 2011, pp. 273–277.

[62] C. Yang, W. Zhu, W. Wang, L. Chen, D. Chen, and J. Cao, "Connectivity-based virtual potential field localization in wireless sensor networks," in *2014 IEEE Wireless Communications and Networking Conference (WCNC)*. IEEE, 2014, pp. 2641–2646.

[63] A. Coluccia and F. Ricciato, "On ml estimation for automatic rss-based indoor localization," in *IEEE 5th International Symposium on Wireless Pervasive Computing 2010*. IEEE, 2010, pp. 495–502.

[64] Y. Wang, "Linear least squares localization in sensor networks," *Eurasip journal on wireless communications and networking*, vol. 2015, no. 1, pp. 1–7, 2015.

[65] W. Navidi, W. S. Murphy Jr, and W. Hereman, "Statistical methods in surveying by trilateration," *Computational statistics & data analysis*, vol. 27, no. 2, pp. 209–227, 1998.

[66] S. Wu, D. Xu, and S. Liu, "Weighted linear least square localization algorithms for received signal strength," *Wireless Personal Communications*, vol. 72, no. 1, pp. 747–757, 2013.

[67] P. M. Santos, T. E. Abrudan, A. Aguiar, and J. Barros, "Impact of position errors on path loss model estimation for device-to-device channels," *IEEE transactions on wireless communications*, vol. 13, no. 5, pp. 2353–2361, 2014.

[68] J. Shirahama and T. Ohtsuki, "Rss-based localization in environments with different path loss exponent for each link," in *VTC Spring 2008-IEEE Vehicular Technology Conference*. IEEE, 2008, pp. 1509–1513.

[69] R. Zemek, D. Anzai, S. Hara, K. Yanagihara, and K.-i. Kitayama, "Rssi-based localization without a prior knowledge of channel model parameters," *International Journal of Wireless Information Networks*, vol. 15, no. 3-4, pp. 128–136, 2008.

[70] U. F. Khan, P. I. Lazaridis, H. Mohamed, R. Albarracín, Z. D. Zaharis, R. C. Atkinson, C. Tachtatzis, and I. A. Glover, "An efficient algorithm for partial discharge localization in high-voltage systems using received signal strength," *Sensors*, vol. 18, no. 11, p. 4000, 2018.

[71] A. Goldsmith, *Wireless communications*. Cambridge university press, 2005.

[72] G. Z. Khan, R. Gonzalez, E.-C. Park, and X.-W. Wu, "Analysis of very high throughput (vht) at mac and phy layers under mimo channel in ieee 802.11 ac wlan," in *2017 19th International Conference on Advanced Communication Technology (ICACT)*. IEEE, 2017, pp. 877–888.

[73] R. L. Haupt, "An introduction to genetic algorithms for electromagnetics," *IEEE Antennas and Propagation Magazine*, vol. 37, no. 2, pp. 7–15, 1995.

[74] I. S. Association *et al.*, "Ieee std 802.11-2016, ieee standard for local and metropolitan area networks—part 11: Wireless lan medium access control (mac) and physical layer (phy) specifications, 2016."

[75] B. L. Welch, "The generalization of student's' problem when several different population variances are involved," *Biometrika*, vol. 34, no. 1/2, pp. 28–35, 1947.

초 록

실내 위치 기반 서비스는 스마트폰을 이용한 실내에서의 경로안내, 스마트 공장에서의 자원 관리, 실내 로봇의 자율주행 등 많은 분야에 접목될 수 있으며, 사물인터넷 응용에도 필수적인 기술이다. 다양한 위치 기반 서비스를 구현하기 위해서는 정확한 위치 정보가 필요하며, 적합한 거리 및 위치를 추정 기술이 핵심적이다. 야외에서는 위성항법시스템을 이용해서 위치 정보를 획득할 수 있다. 하지만 위성항법시스템은 실내에서는 신호가 잘 닿지 않아 이용하기 어렵기 때문에, 실내에서는 위성항법시스템을 대체할 기술이 필요하다.

본 학위논문에서는 와이파이 기반 측위 기술에 대해 다룬다. 구체적으로, 전파의 신호 세기 및 도달 시간을 이용한 정밀한 실내 위치 추정을 위한 세 가지 기술에 대해 다룬다. 먼저, 비가시경로 환경에서의 거리 추정 정확도를 향상시켜 거리 기반 측위의 정확도를 향상시키는 하이브리드 알고리즘을 제안한다. 제안하 알고리즘은 듀얼 밴드 대역의 신호세기를 감쇄량을 측정하여 거리 기반 측위 기법을 적용할 때, 거리 추정부 단계만을 데이터 기반 학습을 이용한 깊은 신경망 회귀 모델로 대체한 방안이다. 적절히 학습된 깊은 회귀 모델의 사용으로 비가시경로 환경에서 발생하는 거리 추정 오차를 효과적으로 감소시킬 수 있으며, 결과적으로 위치 추정 오차 또한 감소시켰다. 제안한 방법을 실내 광선추적 기반 모의실험으로 평가했을 때, 기존 기법들에 비해서 위치 추정 오차를 중간값을 기준으로 22.3% 이상 줄일 수 있음을 검증했다. 추가적으로, 제안한 방법은 실내에서의 AP 위치변화 등에 강인함을 확인했다.

다음으로, 본 논문에서는 비가시경로에서 단일 대역 수신신호세기를 측정했을

때 비가시경로가 많은 실내 환경에서 위치 추정 정확도를 높이기 위한 방안을 제안한다. 단일 대역 수신신호세기를 이용하는 방안은 기존에 이용되는 와이파이, 블루투스, 직비 등의 기반시설에 쉽게 적용될 수 있기 때문에 널리 이용된다. 하지만 신호 세기의 단일 경로손실 모델을 이용한 거리 추정은 상당한 오차를 지녀서 위치 추정 정확도를 감소시킨다. 이러한 문제의 원인은 단일 경로손실 모델로는 실내에서의 복잡한 전파 채널 특성을 반영하기 어렵기 때문이다. 본 연구에서는 실내 위치 추정을 위한 목적으로, 중첩된 다중 상태 경로 감쇄 모델을 새롭게 제시한다. 제안한 모델은 가시경로 및 비가시경로에서의 채널 특성을 고려하여 잠재적인 후보 상태들을 지닌다. 한 순간의 수신 신호 세기 측정치에 대해 각 기준 기지국별로 최적의 경로손실 모델 상태를 결정하는 효율적인 방안을 제시한다. 이를 위해 기지국별 경로손실모델 상태의 조합에 따른 측위 결과를 평가할 지표로서 비용함수를 정의하였다. 각 기지국별 최적의 채널 모델을 찾는데 필요한 계산 복잡도는 기지국 수의 증가에 따라 기하급수적으로 증가하는데, 유전 알고리즘을 이용한 탐색을 적용하여 계산량을 억제하였다. 실내 광선추적 모의실험을 통한 검증과 실측 결과를 이용한 검증을 진행하였으며, 제안한 방안은 실제 실내 환경에서 기존의 기법들에 비해 위치 추정 오차를 약 31% 감소시켰으며 평균적으로 1.92 m 수준의 정확도를 달성함을 확인했다.

마지막으로 FTM 프로토콜을 이용한 실내 위치 추적 알고리즘에 대해 연구하였다. 스마트폰의 내장 관성 센서와 와이파이 통신에서 제공하는 FTM 프로토콜을 통한 거리 추정을 이용하여 실내에서 사용자의 위치를 추적할 수 있다. 하지만 실내의 복잡한 다중경로 환경으로 인한 피크 검출 실패는 거리 측정치에 편향성을 유발한다. 또한 사용하는 디바이스의 종류에 따라 예상치 못한 거리 오차가 발생할 수있다. 본 논문에서는 실제 환경에서 FTM 거리 추정을 이용할 때 발생할 수 있는 오차들을 고려하고 이를 보상하는 방안에 대해 제시한다. 확장 칼만 필터와 결합하여 FTM 결과를 사전필터링 하여 이상값을 제거하고, 거리 측정치의 편향성을 제거하여 위치 추적 정확도를 향상시킨다. 실내에서의 실험 결과 제안한 알고리즘은 거치 측정치의 편향성을 약 44-65% 감소시켰으며 최종적으로 사용자의 위치를 서브미터급으로 추적할 수 있음을 검증했다.

주요어: 거리 기반 측위, 삼변측량, 수신 신호 세기, 실내 위치 추정, 와이파이 측위, Fine Timing Measurement

학번: 2015-20965